Atmos. Chem. Phys., 25, 16679–16695, 2025 https://doi.org/10.5194/acp-25-16679-2025 © Author(s) 2025. This work is distributed under the Creative Commons Attribution 4.0 License.





Measurement report: Anthropogenic activities reduction suppresses HONO formation: direct evidence for secondary pollution control

Mingzhu Zhai^{1,2}, Shengrui Tong¹, Wenqian Zhang³, Hailiang Zhang¹, Xin Li⁴, Xiaoqi Wang⁵, and Maofa Ge¹

¹ State Key Laboratory for Structural Chemistry of Unstable and Stable Species, Beijing National Laboratory for Molecular Sciences (BNLMS), Institute of Chemistry, Chinese Academy of Sciences, Beijing 100190, China ² University of Chinese Academy of Sciences, Beijing 100049, China ³NEAC Key Laboratory of Ecology and Environment in Minority Areas, College of Life and Environmental Sciences, Minzu University of China, Beijing, China ⁴ State Key Joint Laboratory of Environmental Simulation and Pollution Control, College of Environmental Sciences and Engineering, Peking University, Beijing 100871, China

Feking University, Beijing 1008/1, China

Key Laboratory of Beijing on Regional Air Pollution Control,
Faculty of Environment Science and Engineering,
Beijing University of Technology,
Beijing 100124, China

Correspondence: Shengrui Tong (tongsr@iccas.ac.cn) and Maofa Ge (gemaofa@iccas.ac.cn)

Received: 11 June 2025 – Discussion started: 24 July 2025 Revised: 27 October 2025 – Accepted: 27 October 2025 – Published: 25 November 2025

Abstract. Nitrous acid (HONO) is a key precursor of atmospheric hydroxyl radicals (OH) and significantly influences the formation of secondary pollutants, making it essential for understanding and controlling air pollution. While many studies have focused on its formation mechanisms, few have explored the impact of variations in anthropogenic activities on HONO formation. Therefore, we investigated the impact of variations in anthropogenic activities on HONO formation based on comprehensive observations conducted in urban Beijing during autumn and winter of 2022. During clean periods with a 53 % drop in Traffic Performance Index, HONO, CO, and NO₂ levels decreased by 2–3 times compared to polluted periods and significantly lower than previously reported wintertime levels in Beijing. Source apportionment revealed that NO₂ heterogeneous reaction on ground was the dominant HONO source across all periods. Vehicle emissions contributed more to HONO during clean periods, suggesting that reducing anthropogenic activities has a stronger influence on secondary HONO formation. Particulate nitrate (pNO₃) photolysis contributed more to HONO during polluted periods, due to higher pNO₃ fractions in PM_{2.5} under more polluted conditions. Despite including all known formation pathways in the model, unidentified HONO sources still remained. This was strongly associated with intense solar radiation and high OH concentrations at daytime, as well as elevated NH3 concentrations at nighttime. Emission reduction simulations further revealed that a 50 % NO_x reduction during polluted periods could lower HONO by up to 46.3 %, directly demonstrating that reducing anthropogenic activities significantly suppresses HONO formation and provides a scientific basis for the development of air pollution control strategies.

1 Introduction

The worsening global environmental and public health challenges are largely driven by secondary pollution, primarily associated with haze and tropospheric ozone (O₃). This widespread issue poses substantial risks to both human health and food security (Huang et al., 2014; Wang et al., 2024; Achebak et al., 2024; Chen et al., 2024b; Li et al., 2019). Therefore, identifying the key processes controlling the formation of haze and O₃ pollution is critical for improving understanding and informing effective environmental management strategies at the global scale.

The hydroxyl (OH) radicals play a dominant role in secondary pollution (Wang et al., 2023; Tan et al., 2024). Previous studies have found that the photolysis of HONO not only serves as the "trigger" for daytime photochemical reactions in the early morning, but also acts as an important, and even primary source of OH radicals throughout the whole day (Kim et al., 2014; Xue et al., 2016). During more severe pollution, the contribution of HONO to primary OH radicals was higher (70 %–92 %) (Xue et al., 2020; Slater et al., 2020; Xuan et al., 2024). Due to its importance in atmospheric chemistry, the formation mechanisms of HONO have garnered widespread attention (Zhang et al., 2019a; Cui et al., 2018). HONO can be directly emitted into the atmosphere from primary sources, including fossil fuel combustion (Kurtenbach et al., 2001; Liao et al., 2021; Zhang et al., 2022b; Zhang et al., 2022c), biomass burning (Gu et al., 2020; Theys et al., 2020), and agricultural soils (Xue et al., 2024; Bao et al., 2022), all of which are closely related to anthropogenic activities. Secondary formation of HONO involves gas-phase reactions (Pagsberg et al., 1997; Slater et al., 2020), heterogeneous processes on surfaces (Chen et al., 2023; Yang et al., 2021; Wall and Harris, 2017; Zhang et al., 2023c), and photochemical processes (Ye et al., 2017; Jiang et al., 2024; Chen et al., 2024a). The precursors of these processes (e.g., NO, NO₂, and NH₃) also predominantly originate from anthropogenic activities (Yu et al., 2021; Liu et al., 2019a). In summary, anthropogenic activities significantly impact HONO formation. Therefore, understanding how variations in anthropogenic activities affect HONO formation and OH radicals is critical for evaluating the effectiveness of human emission controls and for formulating targeted emission reduction policies.

Policy adjustments and energy structure optimization can significantly affect the characteristics and sources of HONO, as well as its contribution to secondary pollution such as PM_{2.5} and O₃. As the capital of China, Beijing is one of the key areas of air pollution under the supervision of Ministry of Ecology and Environment of the People's Republic of China (Li et al., 2020). Over the past decade, Beijing implemented various measures, including the Clean Air Action Plan in 2013 and the Three-Year Action Plan from 2018 to 2020, and moved many heavy-polluting industries out of Beijing to control industrial pollution (Zhang et al., 2016;

Chan and Yao, 2008). Additionally, the control of vehicle emissions and coal combustion in Beijing was one of the key tasks (Zhang et al., 2016). With the implementation of these policies, PM_{2.5} concentration decreased rapidly, while O₃ concentration increased year by year in Beijing. Moreover, despite the reduction in nitrogen oxides (NO_x) emissions, the particulate nitrate (pNO₃) concentration and its proportion in PM_{2.5} increased (Zong et al., 2022). The air pollution control focus shifted from single PM_{2.5} control to the simultaneous control of both PM_{2.5} and O₃ (Liu et al., 2020; Ye et al., 2023). Stagnant meteorological conditions, such as low wind speeds and high relative humidity, are key drivers of air pollution in autumn and winter. Previous studies have highlighted how such meteorological conditions facilitate the development of secondary pollution in Beijing, with weak southerly winds often driving pollution from industrial regions (Guo et al., 2014; Zheng et al., 2015). In addition, direct anthropogenic emissions, particularly traffic emissions and coal combustions, also are crucial contributors to wintertime PM_{2.5} during haze events in northern Chinese cities (Guo et al., 2013; Shen et al., 2024). Thus, both meteorological stagnation and anthropogenic emissions are the primary drivers of secondary pollution formation in Beijing.

While previous studies have generally focused on HONO source and sink analysis (Xuan et al., 2024; Lin et al., 2022; Jia et al., 2020), limited research has explored the impact of variations in anthropogenic activities on HONO formation and atmospheric oxidation under different pollution conditions. Hereby, we conducted a field observation campaign in urban Beijing from 20 September to 23 December 2022, covering the autumn and winter seasons when O₃ and PM_{2.5} pollution frequently occurred. HONO and related pollutants (NO, NO₂, SO₂, CO, O₃, NH₃, pNO₃, PM_{2.5}, and PM₁₀), as well as meteorological parameters, were simultaneously measured. During this campaign, stagnant meteorological conditions predominated, with low wind speeds and southerly winds. Therefore, the variations in concentration primarily reflected changes in local emissions caused by anthropogenic activities. It provided a unique opportunity to identify HONO sources and their potential impact on secondary pollution formation in urban Beijing, which was rarely studied in the past. In addition, a box model coupled with the Regional Atmospheric Chemistry Mechanism version 2 (RACM2) was used to investigate the chemical budget of HONO under different pollution conditions and to quantify the impact of variations in anthropogenic activities on HONO formation. In summary, through continuous field observations and model simulations, we provide direct evidence that reducing anthropogenic activities is crucial for controlling wintertime HONO formation in Beijing, providing a direct basis for formulating effective air pollution control strategies.

2 Experimental Methods

2.1 Measurement site

The measurement site in this study was on the third floor of NO.2 building at Institute of Chemistry, Chinese Academy of Sciences (ICCAS, 39.99° N, 116.32° E) in Beijing. It is a typical urban site with no obvious industrial or agricultural emission sources. This site is surrounded by dense buildings and main roads, including the North Fourth Ring Road about 500 m to the south of the site and Chengfu Road about 200 m to the north. Therefore, it is heavily influenced by vehicle emissions and anthropogenic activities. More details about the measurement site have been described by previous studies (Hou et al., 2016; Zhang et al., 2023b; Zhang et al., 2019b). The mixing ratios of atmospheric HONO, NH₃, NO, NO₂ and meteorological parameters were measured at ICCAS. In addition, mixing ratios of other trace gases (including O₃, CO and SO₂), PM_{2.5} and PM₁₀ were obtained at the Wanliu monitoring station of the Beijing Environmental Monitoring Station. The Wanliu monitoring station was just about 3 km away from our measurement site in this study, so the atmospheric environment at the two sites was also similar. In addition, photolysis frequencies (j_{O_1D} , j_{NO_2} , j_{HONO}) were acquired simultaneously at Peking University (39.99° N, 116.31° E), which was 600 m to the west of the ICCAS site. The quantitative measurements of pNO₃ in NR-PM₁ were conducted using an Aerodyne Aerosol Chemical Speciation Monitor (ACSM) at Beijing University of Technology (BJUT, 39.87° N, 116.48° E). The BJUT site is located between the southeastern 3rd and 4th ring roads of Beijing, representing a typical urban area similar to the IC-CAS site. The pNO₃ concentration in PM_{2.5} was approximated based on the mass fraction of PM₁ in PM_{2.5}. pNO₃ accounted for 30.56 % of PM_{2.5} mass, which is consistent with the pNO₃ proportion reported in other studies during the same season in the North China Plain (Xiao et al., 2025; Xu et al., 2019). Therefore, the pNO₃ concentrations obtained in this study are reliable for further analysis.

2.2 Measurement instruments

In this study, the mixing ratios of atmospheric HONO was measured by a custom-built HONO analyzer that had been used in previous observations (Zhang et al., 2020; Tong et al., 2016; Hou et al., 2016). The measurement principle of the custom-built HONO analyzer is the same as the commercial long path absorption photometer (LOPAP) (Heland et al., 2001), and the measurement procedure is as follows. HONO is rapidly absorbed by the absorbent solution (0.06 mol L⁻¹ sulfanilamide in 1 mol L⁻¹ HCl) in a double-channel glass spiral coil, forming a stable diazonium salt which then reacts with dye solution (0.8 mmol L⁻¹ N-(1-naphthyl) ethylenediamine-dihydrochloride) to form an azo dye. The azo dye is pumped into the 50 cm liquid waveguide

capillary cell (LWCC) and simultaneously detected by the spectrometer (USB2000+, Ocean Optics, USA), the optical signal is then converted into a numerical value and presented on the computer. Finally, the concentration of HONO is calculated from Lambert's law and the difference of signals between the two channels.

The relevant meteorological parameters such as temperature (Temp), relative humidity (RH), wind speed (WS) and wind direction (WD) were measured by the Vaisala Weather Transmitter (WXT520). The NO_x (NO and NO_2) mixing ratio was measured by a NO_x analyzer (Thermo Scientific, Model 42i) with a detection limit of 1 ppb. The chemiluminescence (CL) technique could overestimate NO_2 concentrations due to interference from NO_y (Villena et al., 2012; Wu et al., 2022a). Details of NO_2 correction were provided in Text S1 of the Supplement. The mixing ratio of NH_3 was measured by an NH_3 analyzer (G2103, Picarro) using Cavity Ring-Down Spectroscopy (CRDS).

2.3 Chemical model

A zero-dimensional photochemical box model (Framework for 0-Dimensional Atmospheric Modeling–F0AM) based on RACM2 that neglects the vertical and horizontal transport processes was used to analyze the HONO budget in this study. The model was constrained by observed chemical species and meteorological parameters, with a time resolution of 1 h. Additionally, an extra 24 h lifetime for all species was defined in the F0AM to prevent the accumulation of secondary species to unreasonable levels. This was achieved by setting a first-order dilution rate of $1/(24 \times 60 \times 60)$ s⁻¹ and setting the background concentration of all species to zero. For more details on this part of the model, refer to Wolfe et al. (2016). The model was run from 20 September to 23 December 2022, with an additional 2 d spin-up on the first day to allow intermediates to reach a steady state.

3 Results and discussion

3.1 Overview of measurement

3.1.1 General analysis of HONO and related air pollutants

Figure 1 illustrates the hourly time series of meteorological parameters and chemical species concentrations during 20 September to 23 December 2022. The specific event between 05:00–23:00 local time (LT) of 12 December was not considered in the further analysis, for the detailed reason given in Text S2 in the Supplement. Throughout the entire campaign, there was a significant variation in Temp and RH due to the span across autumn and winter. However, WS remained at a low level, with a range of 0.18–1.79 m s⁻¹, and the WD was primarily from the southeast and southwest. The meteorological conditions represented typical stagnant conditions that promoted the accumulation of pollutants in Bei-

jing. The HONO concentrations ranged from 0.01–4.79 ppb, with a mean value of 1.21 ± 0.94 ppb. As shown in Table 1, the highest HONO concentration in this study was comparable to or higher than in several previous studies (Hou et al., 2016; Spataro et al., 2013; Li et al., 2021), though still lower than the highest values reported by (Gu et al. 2022). This was because the stagnant conditions contributed to the accumulation of HONO (Shi et al., 2019). However, compared to previous autumn and winter in Beijing, the PM_{2.5} concentration observed in this study was significantly lower, highlighting the effectiveness of air pollution control measures implemented in recent years. General analysis of other pollutants and meteorological parameters were detailed in Text S3 of the Supplement.

According to the National Ambient Air Quality Standards (NAAQS), during the observation period, there were 6 d O₃ pollution where the daily maximum 8h average concentration of O_3 exceeded the Grade II of NAAQS (160 μ g m⁻³, equivalent to 82 ppb at 25 °C and 1013.25 hPa). Additionally, there were more instances of PM2.5 pollution days exceeding the Grade II of NAAQS (75 μ g m⁻³). These days with O₃ pollution were all concentrated between 20 September and 2 October, accompanied by high PM2.5 concentrations (up to $150 \,\mu \mathrm{g \, m^{-3}}$). This represented a typical scenario of concurrent high levels of O₃ and PM_{2.5} pollution frequently observed in cities during autumn (Sun et al., 2009; Qu et al., 2023; Qi et al., 2024), which was associated with meteorological conditions such as relatively high solar radiation intensity, low WS and high RH (Wu et al., 2022b). PM_{2.5} pollution were concentrated between 3 October and 25 November. This period represented the typical periodic cycle of haze pollution observed in urban China during the autumn and winter, linked to stagnant meteorological conditions, including low air diffusion rates and high RH (Cheng et al., 2018; Zhang et al., 2014; Guo et al., 2014; Zhang et al., 2015). The concentration of PM_{2.5} exhibited a typical periodic pattern lasting 4-7 d. Each cycle began with mass concentrations below $10 \,\mu \mathrm{g} \,\mathrm{m}^{-3}$, which then escalated to $100 \,\mu \mathrm{g} \,\mathrm{m}^{-3}$ within 2–5 d, and even exceeded 150 μ g m⁻³. Each PM_{2.5} pollution event consistently extended over 2-4 d, surpassing the Grade II of NAAQS ($75 \,\mu\mathrm{g}\,\mathrm{m}^{-3}$). RH displayed a similar trend to PM_{2.5}. Additionally, the concentrations of HONO, CO, NH₃, and NO₂ progressively increased with the rise in PM_{2.5} levels, suggesting a potential connection between these gaseous pollutants and the formation of PM_{2.5}, consistent with findings from other studies conducted during the same period in autumn and winter (Slater et al., 2020; Wang et al., 2017; Zhang et al., 2023c). The period from 26 November to 23 December was marked by concentrations of gaseous pollutants (HONO, NO, NO₂, CO, NH₃, O₃) and PM_{2.5} which significantly decreased and remained at low levels, the average hourly PM_{2.5} concentration and the daily maximum 8 h average O₃ concentration were less than the Grade I of NAAQS (35 and $100 \,\mu\mathrm{g}\,\mathrm{m}^{-3}$, respectively). In addition, the concentrations of HONO, NO₂, NH₃, and CO were 2–3 times lower compared to the previous two periods. Notably, the atmospheric conditions during this period were unfavorable for pollutant dispersion, characterized by low wind speeds ($< 2 \,\mathrm{m \, s^{-1}}$) and predominantly southerly winds (Fig. S3). However, despite these stagnant meteorological conditions, pollutant concentrations significantly decreased.

Therefore, the observation was segmented accordingly based on the concentrations of O₃ and PM_{2.5}. The period from 20 September to 2 October was characterized by double-high levels of both O₃ and PM_{2.5}, designated as Double-High Pollution Period (DHP, Blue shaded area in Fig. 1). The period from 3 October to 25 November was marked by periodic cycle of PM_{2.5} pollution, identified as the PM_{2.5} Episodic-cycle Pollution Period (PEP, Yellow shaded area in Fig. 1). Based on lower pollutant concentrations, the period from 26 November to 23 December was designated as the Clean Low Pollution Period (CLP, Green shaded area in Fig. 1). This was markedly different from the widespread haze pollution commonly observed in Beijing during December in other studies (Zhang et al., 2019b; Tong et al., 2016), highlighting the uniqueness of this clean period.

3.1.2 Diurnal variation of chemical species across distinct pollution periods with unique characteristics

Meteorological conditions showed typical seasonal transitions from autumn to winter during the DHP, PEP and CLP, characterized by a gradual decrease in Temp and solar radiation, and a delayed sunrise time. RH exhibited an inverse diurnal pattern compared to Temp, and significantly declined during CLP. Detailed diurnal variations of meteorological parameters are provided in Text S3 and Figs. S3-S4 in the Supplement. During the DHP, the peak PM_{2.5} concentration $(60.31 \,\mu\mathrm{g}\,\mathrm{m}^{-3})$ appeared at 04:00 LT, then began to decrease, reaching its lowest value (29.08 μ g m⁻³) at 17:00 LT, and then accumulated again at night (Fig. 2). In contrast, the highest values during the PEP $(52.92 \,\mu \text{g m}^{-3})$ and the CLP $(25.58 \,\mu\mathrm{g}\,\mathrm{m}^{-3})$ both appeared at $20.00 \,\mathrm{LT}$, gradually decreasing at night and reaching their lowest values (41.06 and 12.70 µg m⁻³) at 07:00 LT. Influenced by high solar radiation intensity, intense photochemical reactions led to elevated daytime O₃ concentrations during the DHP. At the same time, higher Temp caused a large emission of volatile organic compounds (VOCs) (Qin et al., 2025; Huangfu et al., 2019; Zhang et al., 2024). The high O₃ concentrations promoted secondary organic aerosols (SOA), pNO₃, pSO₄ and other secondary components through the gas-phase oxidation of VOCs, NO_x , and SO_2 , as well as heterogeneous reactions on particle surfaces, thereby exacerbating PM_{2.5} pollution (Huang et al., 2014; Ji et al., 2024; Tao et al., 2024). Additionally, low WS and high RH under stagnant meteorological conditions further intensified the PM_{2.5} and O₃ synergistic pollution. The PEP represented typical autumn and

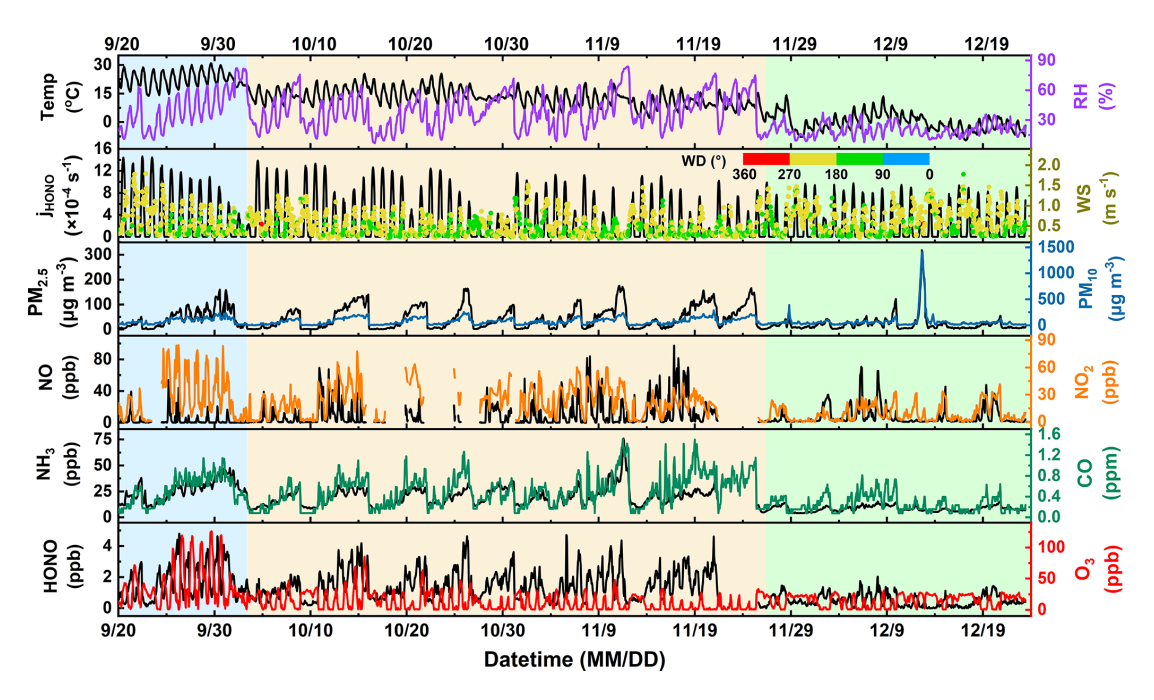


Figure 1. Hourly time series of meteorological parameters (Temp, RH, WS, WD, j_{HONO}) and chemical species (HONO, O₃, NO, NO₂, NH₃, CO, PM_{2.5}, PM₁₀) concentrations from 20 September to 23 December 2022. The blue, yellow and green shades represent DHP, PEP and CLP, respectively. (DHP: Double-High Pollution Period, characterized by double-high levels of both O₃ and PM_{2.5}; PEP: PM_{2.5} Episodic-cycle Pollution Period, characterized by periodic cycle of PM_{2.5} pollution; CLP: Clean Low Pollution Period, characterized by relatively low pollutant concentrations.) The color bar in the second subfigure represents wind direction (WD) in degrees.

Table 1. Comparison of measured HONO at different sites in Beijing urban area.

Location	Sampling periods	HONO (ppb)	HONO _{max} (ppb)	Reference
Beijing, CRAES	13 June-4 July 2019	0.44 ± 0.24	1.39	Li et al. (2021)
Beijing, ICCAS	22 February–2 March 2014	1.84 (Day), 2.06 (Night)	3.24	Hou et al. (2016)
Beijing, ICCAS	1–30 March 2021	1.48 ± 1.09	4.87	Zhang et al. (2023b)
Beijing, PKU	23 January–14 February 2007	1.04 ± 0.73	2.67	Spataro et al. (2013)
	2–31 August 2007	1.45 ± 0.58	2.91	
Beijing, BIPT	18 August–16 September 2018	0.38 ± 0.35	1.87	Xuan et al. (2023)
Beijing, BUCT	1 December 2017–28 February 2018	1.38	_	Lian et al. (2022)
Beijing, CRAES	7–30 May 2017	1.25 ± 0.94	6.69	Gu et al. (2022)
	15–30 January 2018	1.04 ± 1.27	9.55	
Beijing, IAP	25 May-15 July 2018	1.27 ± 0.44	2.41	Liu et al. (2021)
	26 November 2018–15 January 2019	1.13 ± 0.68	3.18	
Beijing, ICCAS	25 October–7 December 2018	2.52 ± 1.61	_	Zhang et al. (2023c)
Beijing, ICCAS	20 September–23 December 2022	1.21 ± 0.94	4.79	This work

winter haze pollution in Beijing, with characteristics similar to those reported in previous haze studies (Shen et al., 2024; Liu et al., 2023). Lower Temp and weaker sunlight reduced photochemical reactions, leading to a significant decrease in O_3 concentrations (Fu et al., 2020), which dropped to one-third of that in the DHP. However, relatively high

 NO_2 concentrations and high RH promoted the formation of pNO₃, which was an important component of PM_{2.5} (Xu et al., 2019). Meanwhile, low WS resulted in weaker diffusion, further contributing to the recurrence of PM_{2.5} pollution (Liu et al., 2023). During the CLP, the relatively small diurnal variation in O₃ concentrations suggested suppressed at-

mospheric photochemistry and a weaker oxidative capacity during this period. In addition, due to lower gaseous pollutant concentrations and lower RH, PM_{2.5} concentration significantly decreased compared to the DHP and PEP. For the diurnal variations of gas pollutants, there were significant differences between the three periods. During the DHP and PEP, traffic-related peaks of NO, NO₂, CO and NH₃ were generally observed during the morning rush hour (07:00-08:00 LT), then generally remained at lower levels throughout the daytime until concentrations began to rise again during the evening rush hour and built up during the night. But the magnitude and subsequent variations differed by species and periods. For example, NO2 and NH3 showed only small enhancements in the PEP, and CO remained elevated after the morning peak during DHP and decreased after 13:00 LT. Notably, the nighttime NO concentration was also very low during the DHP, staying between 0.46-1.17 ppb, which was due to the stronger O₃ consumption of NO (Kurtenbach et al., 2012). During the CLP, the concentrations of NO₂, CO and NH₃ were lower, and their diurnal variation was not obvious. However, they still exhibited a much weaker peak around 08:00-09:00 LT, which indicated a significant reduction in vehicle emissions. The pollution characteristics of the three periods (DHP, PEP, and CLP) exhibited both distinct differences and certain similarities, enabling comparison of the pollution evolution internally among the three periods within this study. In addition, comparisons with other studies conducted during similar periods or seasons in other years helped to highlight the distinct pollution behavior observed in this campaign.

HONO and NO_x (the main precursors of HONO) exhibited similar diurnal variation trends, with higher mixing ratios at night and lower during the day. Specifically, during the DHP and PEP, HONO concentrations significantly peaked at 07:00-08:00 LT (2.71 and 1.86 ppb, respectively) due to nocturnal formation and accumulation as well as direct vehicles emissions in the morning rush hour, then declined due to rapid photolysis in the daytime. Subsequently, due to the absence of photolysis reactions and the arrival of the evening rush hour, the HONO concentration began to accumulate, remaining at a high level throughout the night (1.94–2.33 and 1.67–1.81 ppb, respectively). This phenomenon was also observed in previous studies during PM_{2.5} and O₃ pollution in autumn and winter in Beijing (Jia et al., 2020; Li et al., 2021; Liu et al., 2021), which indicated that HONO was a crucial precursor in driving the formation of PM_{2.5} and O₃ pollution. Due to the difference in sunrise time and photolysis processes, the peak HONO concentration during the PEP occurred 1 hour later in the morning compared to the DHP. Wang et al. also observed that the decline in HONO concentration varied seasonally with sunrise times, being around 08:00 LT in winter, around 07:00 LT in autumn, and around 6:00 LT in summer and spring (Wang et al., 2017). During the CLP, the HONO concentration significantly decreased and remained at low level (0.28–0.66 ppb). Due to nighttime formation and accumulation, the HONO concentration peaked (0.66 ppb) around midnight, then slowly decreased before sunrise. The HONO concentration did not show a significant increase during the morning rush hour (07:00–08:00 LT), indicating a substantial reduction in vehicle emissions during the CLP. The HONO concentration decreased to its minimum value (0.28 ppb) at 11:00 LT, then showed an increase around noon, reaching 0.33 ppb at 13:00 LT. Subsequently, HONO began to accumulate again as the sunlight intensity weakened, maintaining levels between 0.55–0.66 ppb throughout the night.

In summary, the DHP and PEP represented common pollution scenarios during the autumn and winter in Beijing, with HONO concentration levels and diurnal variation comparable to those reported in previous studies (Liu et al., 2021; Zhang et al., 2023a; Slater et al., 2020). However, the CLP observed in this study, which occurred during the frequent winter haze pollution period (26 November to 23 December), differed significantly from the pollution situation in the Beijing urban area during the same period in other studies. For example, Tong et al. (2016) observed PM_{2.5} pollution events (with average $PM_{2.5}$ concentrations up to $144 \,\mu g \,m^{-3}$) accompanied by high HONO concentrations (3 ppb) in urban Beijing from 12 to 22 December 2015. Zhang et al. (2019b) captured a severe haze period with PM2.5 concentrations reaching 418 µg m⁻³ and HONO concentrations reaching 5.8 ppb at the same site from 16 to 24 December 2016, while a clean period brought by strong winds was also observed. Liu et al. (2021) also observed haze pollution in urban Beijing in December 2018. Further analysis revealed that the Traffic Performance Index (TPI) in Beijing was relatively low at 3.01 in December 2022, significantly lower than usual, indicating reduced vehicle emissions accompanied by a significant decrease in anthropogenic activities. Compared to September, October, and November 2022, the TPI decreased by 53 %, 41 %, and 25 %, respectively. Compared to December 2021, the decrease was as high as 55 % (https://www.bjtrc.org.cn/List/index/cid/7.html, last access: 14 June 2024). These findings demonstrated that even under stagnant regional meteorological conditions, a substantial reduction in direct anthropogenic activities could lead to significant air quality improvements, resulting in cleaner period. Considering the rapid urbanization in China and the sharp increase in vehicle ownership, these findings may also be applicable to other cities or highly industrialized regions, offering valuable insights for formulating scientifically effective emission reduction policies. The following sections will further explore the source contributions of HONO under different pollution scenarios and quantify the specific impact of direct emission reductions on improving PM_{2.5} and O₃ pollution.

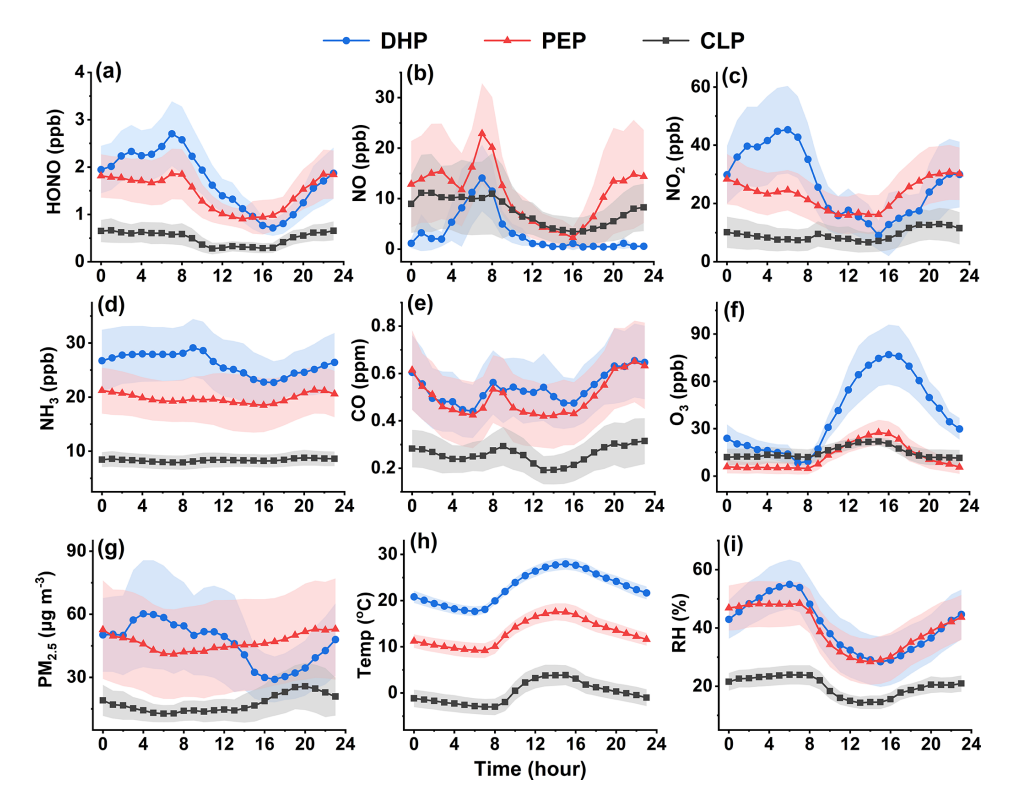


Figure 2. The diurnal variations of chemical species (HONO, NO, NO₂, NH₃, CO, O₃, PM_{2.5}) and meteorological parameters (Temp, RH) during three periods. The blue, red, and black dotted lines represent the mean hourly values for DHP, PEP and CLP, respectively. The shaded areas represent half of the standard deviations ($\pm 0.5\sigma$).

3.2 HONO budget during nighttime

Vehicle emissions are the most important direct source of HONO in urban areas (Xu et al., 2015; Yun et al., 2017; Yin et al., 2023). As described in diurnal variations and previous studies, CO and NO were major pollutants originating from combustion processes and could be directly emitted into the atmosphere through vehicle emissions in urban areas (Sun et al., 2014; Bond et al., 2013). HONO exhibited a positive correlation with NO or CO, indicating that vehicle emissions played an important role in HONO formation at this observation site (Fig. S5). However, it is noteworthy that during the DHP and PEP, which had higher TPI values, the correlation between HONO and NO or CO was lower than that in the CLP. The higher intensity of anthropogenic activities in these periods led to a significant increase in PM_{2.5} and NO₂ concentrations, which in turn enhanced the secondary formation of nighttime HONO (e.g., NO₂ heterogeneous reaction on various surfaces), making it the dominant process. In contrast, the lower PM_{2.5} concentrations weaken the contribution of secondary HONO formation during the CLP, resulting in a more pronounced correlation between vehicle emissions and nighttime HONO formation (Jia et al., 2020). To assess the impact of vehicle emissions in this observation period, the local emission factor EF_{emis} (= $\Delta HONO / \Delta NO_x$) was derived based on ambient measurements. As described in Text S4 and Table S2 in the Supplement, the minimum EF_{emis} (0.0051) in fresh plumes was taken as the upper limit for the direct emission factor to minimize the influence of secondary HONO formation (Su et al., 2008), which was comparable to the value of 0.0051 measured in Beijing (Zhang et al., 2022c), 0.0053 measured in Ji'nan (Li et al., 2018a) and 0.005 measured in Hong Kong (Xu et al., 2015). Since the types of vehicles around this site had not changed, it was reasonable to use the same EF_{emis} (0.0051) to assess the contribution of vehicle emission to the HONO through the entire observation period. As shown in Fig. 3a, the directly emitted HONO (HONO_{emis}) exhibited distinct nighttime patterns among the three periods. HONO_{emis} steadily increased over night in DHP, suggesting continuous accumulation driven by persistent vehicle emissions and reduction in boundary layer height. During the PEP, HONO_{emis} remained relatively stable at nighttime and modest increased during both the evening (\sim 19:00 LT) and early morning (\sim 06:00 LT) rush hours, reflecting enhanced traffic activity. HONO_{emis} during the CLP was markedly lower than in DHP and PEP, remained at low levels over night, indicating weaker vehicle emission. Although HONO_{emis} were relatively high during the DHP and PEP (Fig. 3a), the contribution of direct emissions was lower than that in the CLP, due to the greater influence of other

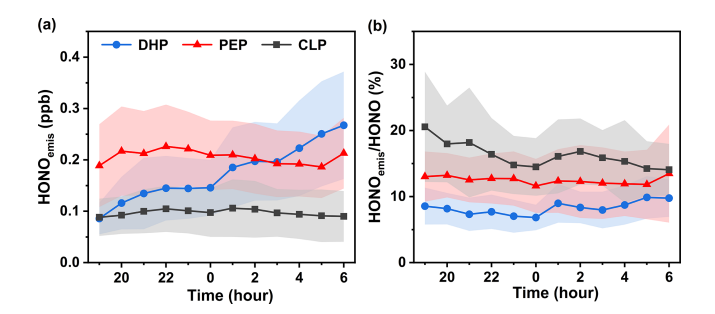


Figure 3. The hourly variations of (a) HONO_{emis} and (b) HONO_{emis} / HONO at nighttime during three periods. The blue, red, and black dotted lines represent the mean hourly values for DHP, PEP and CLP, respectively. The shaded areas represent half of the standard deviations ($\pm 0.5\sigma$).

sources. Vehicle emissions accounted for 8.3 %, 12.5 %, and 16.3 % of nighttime HONO during the DHP, PEP, and CLP, respectively, indicating that the relative importance of direct emissions increases under cleaner periods, which was consistent with previous studies (Jia et al., 2020; Zhang et al., 2022c).

The heterogeneous reactions of NO₂ on various surfaces were widely recognized as the primary secondary source of HONO (Spataro and Ianniello, 2014; Kebede et al., 2016; Indarto, 2011). To mitigate the influence of direct emissions, HONOcorr (HONO-HONOemis) was utilized for further analysis. The HONOcorr / NO2 ratio was often used to represent the heterogeneous conversion fraction of NO2 to HONO due to its first-order dependence on NO₂ (Li et al., 2012; Jenkin et al., 1988). The HONOcorr / NO2 ratio in DHP, PEP, and CLP were 0.114, 0.086, and 0.085, respectively, which were higher than previous studies (Zhang et al., 2023c, 2022b; Cui et al., 2018). This indicated that the potential for heterogeneous conversion from NO₂ to HONO was stronger during this observation period, especially in DHP. The dominant medium for the heterogeneous conversion of NO₂ has been a contentious issue whether aerosol surfaces or ground surfaces are more important. Due to the absence of measurements of aerosol surface density (SA) in this observation period, PM_{2.5} concentrations were used as a substitute to determine the impact of aerosols on the conversion of NO₂ to HONO at nighttime (Lu et al., 2018; Cai et al., 2017). The relationship of HONOcorr with NO₂ and $NO_2 \times PM_{2.5}$ was demonstrated in Fig. S7. HONO_{corr} exhibited a significant positive correlation with NO2, with correlation coefficients (R^2) of 0.66, 0.45, and 0.38 during the DHP, PEP, and CLP, respectively, indicating that the heterogeneous reaction of NO2 was an important source of HONO in this observation period. Additionally, the R^2 between $HONO_{corr}$ and $NO_2 \times PM_{2.5}$ was 0.72, 0.48, and 0.35 for the three periods, suggesting that the heterogeneous reaction of NO2 on aerosol contributed to HONO formation during the DHP and PEP, which was closely associated with the higher PM_{2.5} concentrations providing more reactive surfaces. However, compared to previous studies conducted in Beijing during autumn and winter, the correlation between $HONO_{corr}$ and $NO_2 \times PM_{2.5}$ during the DHP and PEP was significantly lower (Tong et al., 2015; Nie et al., 2015). For example, (Yan et al., 2015) and (Zhang et al., 2019b) reported that during haze pollution events in Beijing in the mid-2010s, the average PM_{2.5} concentration could reach approximately $130 \,\mu g \, m^{-3}$, with levels during severe haze episodes approaching 311 μ g m⁻³. In contrast, the average PM_{2.5} concentration during the DHP and PEP in this study was only around $46 \,\mathrm{ug}\,\mathrm{m}^{-3}$. This discrepancy may be attributed to the implementation of air pollution control policies in recent years, which led to a substantial reduction in PM2.5 concentrations in Beijing compared to previous years (Huang et al., 2021; Guha et al., 2024), thereby limiting the heterogeneous reactions of NO2 on aerosols. Particularly during the CLP, PM_{2.5} concentrations decreased by 63 % compared to the DHP and PEP, further weakening the role of aerosol in NO₂ heterogeneous reactions to produce HONO. Consequently, compared to NO₂ heterogeneous reactions on ground surfaces, its reaction on aerosol played a more limited role in HONO formation. Notably, HONOcorr exhibited the strongest correlation with both NO_2 and $NO_2 \times PM_{2.5}$ during the DHP, likely due to enhanced oxidation of organic and inorganic components, consistent with the high O₃ concentrations observed, which altered the surface reactivity and consequently promoting NO₂ conversion to HONO (George et al., 2015; Ndour et al., 2008).

It was observed that the HONO_{corr} / NO₂ ratios increased with the increase in RH (< 70%), indicating that the absorbed water on the surface participated in the heterogeneous reactions of NO2 to HONO (Stutz et al., 2004). Furthermore, once RH exceeded a critical threshold (≥ 70 %) (Dark blue dots in the Fig. S7a-b), the heterogeneous reactions of NO₂ on various surfaces were inhibited, leading to a decrease in HONO_{corr} / NO₂ with increasing RH. Similar segmented correlations between HONOcorr and RH had been observed in previous studies, which had been interpreted as evidence of the nonlinear dependence of NO₂ to HONO conversion efficiency on RH (Qin et al., 2009; Li et al., 2012; Tong et al., 2015). One possible explanation was that the quantity of water layers formed on various surfaces rapidly increased with rising RH, resulting in effective uptake of HONO and making the surfaces less accessible or reducing their reactivity with NO₂ (Yu et al., 2022; Li et al., 2021).

3.3 Model simulations for HONO sources and sinks

The base sources of HONO in the model simulation only included the homogeneous reaction of NO with OH ($S_{\rm NO+OH}$), while the sinks of HONO included the dry deposition of HONO ($L_{\rm dep}$), the photolysis of HONO ($L_{\rm photo}$), and the homogeneous reaction of HONO with OH ($L_{\rm HONO+OH}$). The base model could only explain 4.2 %, 19.1 %, and 19.0 % of

the observed HONO (HONO_{obs}) during the DHP, PEP, and CLP, respectively, which led to an underestimation of OH and O₃ concentrations in the atmosphere (Liu et al., 2019b; Tie et al., 2019). The proportion of soil near the site was minimal and primarily used for landscaping, with almost no fertilization activities. Moreover, the NH₃ concentration was significantly lower than that observed in rural areas of North China where soil emissions were considered (Xue et al., 2021). Therefore, soil emissions were not included in the model. Other known sources of HONO were incorporated into the model simulations, including vehicle direct emissions (S_{eims}), the heterogeneous reactions of NO₂ on ground surfaces $(S_{\text{NO}_{2_g}})$ and aerosol surfaces $(S_{\text{NO}_{2_a}})$, the photo-enhanced heterogeneous reactions of NO2 on ground surfaces $(S_{NO_{2,n},hv})$ and aerosol surfaces $(S_{NO_{2,n},hv})$, as well as the photolysis of pNO₃ ($S_{pNO_3 hv}$). The parameterization mechanisms for the production and removal pathways of HONO were detailed in Table 2, and the specific parameter values were presented in Text S6 of the Supplement.

After incorporating all HONO sources listed in Table 2, the diurnal variation of simulated HONO (HONO_{sim.0}) from different sources was illustrated in Fig. 4. The heterogeneous reaction of NO₂ on ground (including $S_{NO_{2g}}$ and $S_{NO_{2g},hv}$) was the main source of HONO during the observations, contributing 45.5 %, 37.8 %, and 44.0 % to HONO_{sim,0} in DHP, PEP, and CLP, respectively. The heterogeneous reaction of NO_2 on aerosol surfaces (including S_{NO_2} and S_{NO_2} and S_{NO_2} contributed 16.7 %, 14.9 %, and 10.5 % to HONO_{sim,0} reflecting the variation in PM_{2.5} concentrations across the three periods (Table S1 in the Supplement). The heterogeneous reactions of NO₂ (on ground and aerosol surfaces) contributed over 50 % of HONO_{sim,0}, comparable to previous research, 54.4% in the Yangtze River Delta region (Shi et al., 2020), and 63 % in urban areas of Beijing (Zhang et al., 2023b). pNO₃ photolysis contributed 12.7 %, 11.7 %, and 5.0 % to HONO_{sim.0} during the DHP, PEP, and CLP, respectively. Although traditionally considered minor (Xue et al., 2020; Zhang et al., 2022c), our results suggested that its importance increases under more polluted conditions, consistent with the higher nitrate fractions observed in PM_{2.5} composition studies (Zhai et al., 2021; Xu et al., 2019; Xiao et al., 2025). While still lower than the 31 %-36 % reported in southern China (Fu et al., 2019), pNO₃ photolysis remained a non-negligible source. A sensitivity analysis (Text S6 and Table S3) showed that variations in the enhancement factor (EF) had a limited effect on HONO formation when EF = 3, but led to a noticeable increase when EF = 300, indicating that EF could influence the contribution of pNO₃ photolysis to HONO production. These results highlight the importance of EF in quantitatively constraining the HONO budget. The homogeneous reaction of NO with OH radicals typically peaked around 08:00-09:00 LT, contributing 8.2 %, 22.5 %, and 21.1 % during the three periods. Vehicle emissions accounted for 17.0 %, 13.0 %, and 19.5 % with a relatively higher contribution during cleaner periods, consistent with previous studies (Jia et al., 2020). Despite including all known sources, a notable portion of $HONO_{obs}$ remained unexplained. The unknown HONO concentration ($HONO_{unknown} = HONO_{obs} - HONO_{sim,0}$) accounted for 50.4 %, 16.9 %, and 7.0 % during the three periods, respectively. Notably, the $HONO_{unknown}$ / $HONO_{obs}$ increased with pollution severity (higher $PM_{2.5}$ and O_3), suggesting the existence of additional unidentified sources or processes under complex pollution conditions. Overall, while the model captures the major known sources of HONO, the high proportion of unexplained HONO during heavily polluted periods highlights the need for further investigation into missing mechanisms.

To further investigate the formation mechanisms of HONO_{unknown}, this study employed a time-segmented analysis approach. The transitional periods between day and night (i.e., three hours before and after sunrise and sunset) were excluded, then separately analyzing representative daytime (10:00–15:00 LT) and nighttime (22:00–03:00 LT) episodes. This time-segmented analysis approach effectively avoided the interference of diurnal transitions, allowing for a clearer distinction of the characteristics of HONO_{unknown} during different episodes. Due to the rapid photolysis of HONO around noontime, the production rate of HONO_{unknown} (*P*_{unknown}) during the daytime could be expressed by the following equation:

$P_{\text{unknown}} = \text{HONO}_{\text{unknown}} \times j_{\text{HONO}}$

 P_{unknown} exhibited a positive correlation with OH \times j_{HONO} , with R^2 of 0.69 (Fig. S9), suggesting that daytime HONO_{unkonwn} might act as a sink for OH radicals. This result was consistent with our previous studies conducted through ground (Lin et al., 2022; Zhang et al., 2023b) and vertical observations (Zhang et al., 2020) in urban Beijing. Through linear regression analysis of nighttime HONO_{unknown} with other pollutants and meteorological parameters, significant positive correlations between HONO_{unknown} and RH, NO₂, PM_{2.5}, NH₃, and CO were observed (Fig. S10). Given the strong correlations between CO and PM_{2.5} (R^2 = 0.54) and NH₃ ($R^2 = 0.59$), these pollutants were likely to share common sources, which could explain the observed good correlation between CO and HONO_{unknown}. Further multivariate linear regression analysis revealed that, compared to individual pollutants, the composite parameter $NO_2 \times NH_3 \times RH$ exhibited a significantly stronger correlation with HONO_{unknown}. This finding suggested that HONO_{unknown} may be related to NH₃-promoted heterogeneous reactions of NO₂, with RH playing a crucial role in this process. Li et al. (2018b) proposed that NH₃ could promote the hydrolysis of NO2 at the air-water interface to produce HONO, which could be an important pathway for HONO production in NH₃-rich environments. Additionally, our group's previous research on haze pollution during the autumn and winter of 2018 demonstrated that the synergistic

*J*HONO

 $k_{\text{OH+HONO}}$ $k = \frac{v_{\text{HONO}}}{\text{BLH}}$

 $L_{\rm photo}$

 L_{dep}

 $L_{\text{HONO+OH}}$

Source (S)/Loss (L)	RACM Mechanisms	Parametrization
$S_{ m emis}$	Direct emission	$EF_{emis} = 0.0051$
$S_{ m NO+OH}$	$NO + OH \rightarrow HONO$	$k_{ m OH+NO}$
$S_{\mathrm{NO}_{2_g}}$	$2NO_2 + H_2O \xrightarrow{ground surface} HONO + HNO_3$	$k_{\text{het-g}} = \frac{1}{8} \times v_{\text{NO}_2} \times \frac{1}{\text{MLH}} \times \gamma_{\text{g}}$
$S_{\mathrm{NO}_{2_a}}$	$2NO_2 + H_2O \xrightarrow{aerosol \ surface} HONO + HNO_3$	$k_{\text{het-a}} = \frac{1}{8} \times v_{\text{NO}_2} \times \text{SA} \times \gamma_a$
$S_{\mathrm{NO}_{2_g},hv}$	$2NO_2 + H_2O + hv \xrightarrow{ground surface} HONO + HNO_3$	$k_{\text{het-g},hv} = \frac{1}{4} \times v_{\text{NO}_2} \times \frac{1}{\text{MLH}} \times \gamma_{\text{g},hv} \times \frac{j_{\text{NO}_2}}{0.005 \text{s}^{-1}}$
$S_{ ext{NO}_{2_a},hv}$	$2NO_2 + H_2O + hv \xrightarrow{aerosol \ surface} HONO + HNO_3$	$k_{\text{het-a},hv} = \frac{1}{4} \times v_{\text{NO}_2} \times \text{SA} \times \gamma_{\text{a},hv} \times \frac{j_{\text{NO}_2}}{0.005 \text{s}^{-1}}$
$S_{\mathrm{pNO}_3,hv}$	$pNO_3 + hv \rightarrow 0.67HONO + 0.33NO_x$	$k_{\text{pNO}_3,hv} = \text{EF} \times j_{\text{HNO}_3}$

Table 2. Parameterized HONO production/loss mechanisms in model simulations.

 $HONO + hv \rightarrow OH + NO$

HONO deposition

 $HONO + OH \rightarrow NO_2 + H_2O$

As shown in Text S5 of the Supplement, the values of γ_g and $\gamma_{g,hv}$ were set to 2.94×10^{-6} , while the values of γ_a and $\gamma_{a,hv}$ were set to 3.12×10^{-5} . MLH was taken as 50 m in this observation to assess the ground-level sources of HONO (Lee et al., 2016; Xue et al., 2020, 2022). The EF was set to 30, a value commonly used in field observations conducted in autumn in Beijing (Zhang et al., 2022a; Xuan et al., 2024). The average dry deposition velocity of HONO (v_{HONO}) was taken as $2 \, \mathrm{cm \, s^{-1}}$ (Harrison et al., 1996). S_{NO+OH} , $S_{OH+HONO}$, and j_{HNO_3} were calculated in the RACM mechanisms. BLH represents boundary layer height, with units in meters (m).

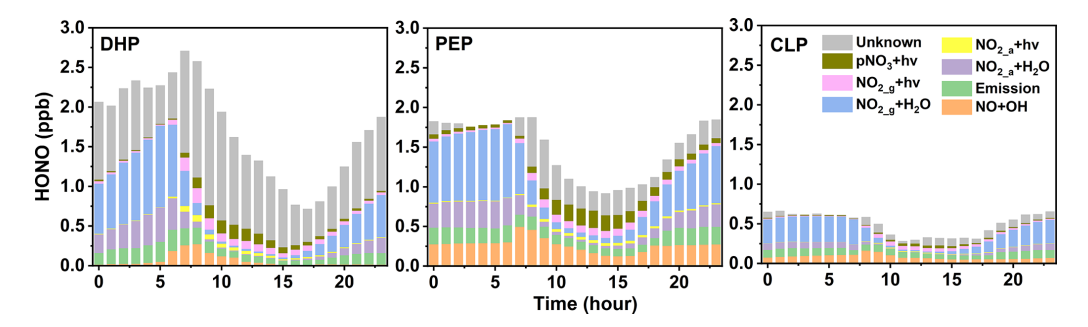


Figure 4. The diurnal variations of the HONO_{sim.0} from different sources during the DHP, PEP and CLP.

effect of RH and NH3 significantly enhanced the NO2 heterogeneous conversion to HONO, leading to a positive feedback mechanism between haze pollution and HONO production (Zhang et al., 2023c). Notably, RH and NO2 levels at nighttime in the DHP and PEP were comparable to those observed during haze pollution episodes in the autumn and winter of 2018. Therefore, the enhancement factor ($f_{NH_2,RH}$) from Zhang et al. (2023c) work for nighttime HONO production in the model simulation was applied. Since RH remained consistently below 40 % during the CLP, f_{NH3.RH} was set to 1. Additionally, an extra HONO source, enhanced by photolysis and consuming OH radicals, was introduced for daytime HONO production during the three periods. The revised simulation results (HONO_{sim.1}) showed good agreement with HONO_{obs}, successfully reproducing the HONO variations during the three periods (Fig. 5). Due to intermittent light rain, the model exhibited slightly reduced performance during certain periods, such as on 22 September and 3 October. These findings have important implications for future studies. First, pathways related to solar radiation and OH radicals should be considered in future studies on daytime HONO sources, as also suggested by recent findings using explainable machine learning approaches (Gao et al., 2024). Second, for typical pollution events characterized by high relative humidity (RH > 40 %) and elevated NH₃ concentrations (> 10 ppb), the synergistic effect of RH and NH₃ in promoting NO₂ heterogeneous reactions at the air-water interface should be fully considered. These insights provide a critical basis for improving parameterization schemes of HONO formation mechanisms in atmospheric chemistry models.

As mentioned in the "Overview of measurement", the TPI in December decreased by approximately 50% compared to September and October, reflecting a significant reduction in anthropogenic activities. To directly assess the

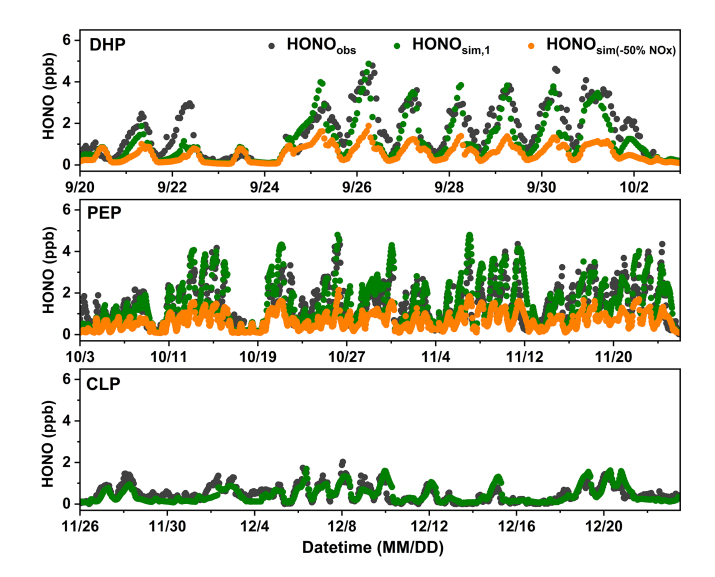


Figure 5. Time series of observed HONO and simulated HONO under different scenarios during the DHP, PEP, and CLP. The black scatter points represent observed HONO (HONO_{obs}), the green scatter points represent the revised simulated HONO (HONO_{sim,1}), the orange scatter points represent simulated HONO after a 50 % reduction in NO_x emissions (HONO_{sim(-50 % NO_x)}). The data had a temporal resolution of 1 h.

impact of reduced anthropogenic activities on atmospheric HONO, we assumed a 50 % reduction in NO_x emissions during the DHP and PEP due to decreased anthropogenic activities. This NO_x reduction scenario was incorporated as a constraint in the model to obtain simulated HONO concentrations (HONO_{sim(-50%NO_x)). The simulation results (or-} ange scatter points in Fig. 5) indicated that NO_x reduction led to significant reductions in HONO levels, with declines of 42.7 % and 46.3 % during the DHP and PEP, respectively. These quantitative results confirmed that reduced anthropogenic activities could effectively suppress atmospheric HONO formation, thereby positively contributing to improved air quality. In summary, this study provided the first direct evidence through scenario simulations that reducing anthropogenic activities was a key strategy for controlling atmospheric HONO levels in autumn and winter in Beijing, thereby limiting the formation of secondary pollutants such as PM_{2.5} and O₃. These findings offered important scientific support for formulating effective pollution control strategies.

4 Conclusions

Here, we presented measurements of HONO in urban Beijing during the autumn and winter of 2022, combined with a box model based on RACM2 to analyze its variation patterns and source mechanisms under three typical pollution periods. Particular attention was given to unidentified HONO sources and their implications for atmospheric chemistry.

Our study identified three distinct pollution scenarios: Double-High Pollution period of O₃ and PM_{2.5} (DHP), PM_{2.5} Episodic-cycle Pollution period (PEP), and Clean Low Pollution period (CLP). Notably, stagnant meteorological conditions predominated, characterized by low wind speeds and southerly winds, suggesting that variations in pollutant concentrations were mainly driven by local emissions associated with anthropogenic activities. The HONO variation characteristics exhibited similarities and differences across the three periods. The average HONO concentrations were 1.71 and 1.46 ppb during the DHP and PEP, respectively, while it decreased more than threefold to 0.50 ppb during the CLP. HONO exhibited similar diurnal variation trends in the three periods, with higher mixing ratios at night and lower during the day. Other pollutants (NO₂, NH₃, CO, and PM_{2,5}) also showed significantly lower levels (2-3 times) during the CLP compared to the DHP and PEP, while NO concentrations were lowest during the DHP. O₃ concentration was highest during the DHP and were similar during the PEP and CLP. The differences in pollutant concentration were related to the distinct HONO formation mechanisms and conversion frequencies during the three periods, reflecting the variations in atmospheric chemical processes.

The contribution of vehicle emission to nighttime HONO was highest during the CLP. During the DHP and PEP, stronger correlations between nighttime HONO with PM_{2.5} and NO2 indicated a relative greater contribution from heterogeneous reactions, thereby reducing the relative impact of vehicle emission. The NO2 heterogeneous reaction on ground was the dominant HONO source in all periods, contributing 45.5 %, 37.8 %, and 44.0 % of simulated HONO, respectively. NO₂ heterogeneous reactions on aerosol surfaces contributed 16.7 %, 14.9 %, and 10.5 % in all periods, respectively. pNO₃ photolysis accounted for 12.7 %, 11.7 %, and 5.0 %, consistent with PM_{2.5} concentrations in the three periods. The homogeneous reaction of NO with OH contributed 8.2 %, 22.5 %, and 21.1 %, respectively. Notably, although overall anthropogenic emissions were lower during the CLP, the relative contribution of vehicle emissions to HONO became more significant. Despite incorporating all known sources into the model, significant missing HONO sources remained during the three periods, accounting for 50.4 %, 16.9 %, and 7.0 %, respectively. Correlation analysis indicated that daytime HONO_{unknown} was associated with solar radiation and OH radical consumption, while nighttime HONO_{unknown} was related to NH₃-promoted heterogeneous reactions of NO₂. Including these pathways in the model significantly improved the agreement with observed HONO. Based on TPI and scenario simulations, a 50% reduction in NO_x emissions due to decreased anthropogenic activities during the DHP and PEP would lead to a 42.7 % and 46.3 % decrease in HONO concentrations, respectively. These results had important policy implications for air pollution control. The study indicated that controlling vehicle emissions might be an effective measure to reduce HONO concentrations and improve air quality. However, during haze pollution periods, it is necessary to complement vehicle emission control with integrated multi-source measures, such as reducing NO₂ and NH₃ emissions, to limit the secondary formation of HONO and thereby more effectively reduce air pollution.

In summary, based on comprehensive observations and model simulations of HONO in Beijing during the autumn and winter, this study elucidated the primary source characteristics of HONO under different typical pollution periods and quantitatively assessed the direct impact of variations in anthropogenic activities on its formation. The results highlighted the critical role of controlling anthropogenic emissions in improving air quality and provided strong scientific support for formulating effective air pollution control strategies in urban areas. However, this study focused on urban environments during the autumn and winter, and a systematic understanding of how variations in anthropogenic activities influence HONO in suburban and rural regions remains lacking. Future research should integrate multi-site and multiseasonal observations with laboratory studies and regional chemical transport modeling to improve our understanding of HONO sources and atmospheric chemistry, and to quantitatively evaluate the impact of variations in anthropogenic activities on air quality across different environments.

Data availability. The data presented in this study can be accessed through https://doi.org/10.5281/zenodo.16083849 (Zhai et al., 2025).

Supplement. The supplement related to this article is available online at https://doi.org/10.5194/acp-25-16679-2025-supplement.

Author contributions. ZMZ contributed to methodology, data curation and analysis, and original draft writing. TSR contributed to conceptualization, investigation, data curation, writing, review and editing, supervision, and funding acquisition. ZWQ and ZHL contributed to data analysis, result discussion, and manuscript commenting. LX and WXQ participated in observational studies and data curation. GMF contributed to conceptualization, investigation, manuscript review, supervision, and funding acquisition.

Competing interests. The contact author has declared that none of the authors has any competing interests.

Disclaimer. Publisher's note: Copernicus Publications remains neutral with regard to jurisdictional claims made in the text, published maps, institutional affiliations, or any other geographical representation in this paper. While Copernicus Publications makes every effort to include appropriate place names, the final responsibility lies with the authors. Views expressed in the text are those of the authors and do not necessarily reflect the views of the publisher.

Financial support. This work was supported by the National Natural Science Foundation of China (contract nos. 42430606, W2521034).

Review statement. This paper was edited by Eleanor Browne and reviewed by Dianming Wu and one anonymous referee.

References

- Achebak, H., Garatachea, R., Pay, M. T., Jorba, O., Guevara, M., Pérez García-Pando, C., and Ballester, J.: Geographic sources of ozone air pollution and mortality burden in Europe, Nat. Med., 30, 1732–1738, https://doi.org/10.1038/s41591-024-02976-x, 2024.
- Bao, F., Cheng, Y., Kuhn, U., Li, G., Wang, W., Kratz, A. M., Weber, J., Weber, B., Poschl, U., and Su, H.: Key Role of Equilibrium HONO Concentration over Soil in Quantifying Soil-Atmosphere HONO Fluxes, Environ. Sci. Technol., 56, 2204–2212, https://doi.org/10.1021/acs.est.1c06716, 2022.
- Bond, T. C., Doherty, S. J., Fahey, D. W., Forster, P. M., Berntsen, T., DeAngelo, B. J., Flanner, M. G., Ghan, S., Kärcher, B., Koch, D., Kinne, S., Kondo, Y., Quinn, P. K., Sarofim, M. C., Schultz, M. G., Schulz, M., Venkataraman, C., Zhang, H., Zhang, S., Bellouin, N., Guttikunda, S. K., Hopke, P. K., Jacobson, M. Z., Kaiser, J. W., Klimont, Z., Lohmann, U., Schwarz, J. P., Shindell, D., Storelvmo, T., Warren, S. G., and Zender, C. S.: Bounding the role of black carbon in the climate system: A scientific assessment, J. Geophys. Res. Atmos., 118, 5380–5552, https://doi.org/10.1002/jgrd.50171, 2013.
- Cai, R., Yang, D., Fu, Y., Wang, X., Li, X., Ma, Y., Hao, J., Zheng, J., and Jiang, J.: Aerosol surface area concentration: a governing factor in new particle formation in Beijing, Atmos. Chem. Phys., 17, 12327–12340, https://doi.org/10.5194/acp-17-12327-2017, 2017.
- Chan, C. K. and Yao, X.: Air pollution in mega cities in China, Atmos. Environ., 42, 1–42, https://doi.org/10.1016/j.atmosenv.2007.09.003, 2008.
- Chen, J., Jiang, H., Chen, X., Wang, J., Huang, D., Lian, C., Wang, W., Ammann, M., Bao, F., Chen, C., and Zhao, J.: A Novel Mechanism for NO₂-to-HONO Conversion on Soot: Synergistic Effect of Elemental Carbon and Organic Carbon, Environ. Sci. Technol. Lett., https://doi.org/10.1021/acs.estlett.3c00624, 2023.
- Chen, T., Ren, Y., Zhang, Y., Ma, Q., Chu, B., Liu, P., Zhang, P., Zhang, C., Ge, Y., Mellouki, A., Mu, Y., and He, H.: Additional HONO and OH Generation from Photoexcited Phenyl Organic Nitrates in the Photoreaction of Aromatics and NO_x, Environ. Sci. Technol., https://doi.org/10.1021/acs.est.3c10193, 2024a.
- Chen, Z.-Y., Petetin, H., Méndez Turrubiates, R. F., Achebak, H., Pérez García-Pando, C., and Ballester, J.: Population exposure to multiple air pollutants and its compound episodes in Europe, Nat. Commun., 15, 2094, https://doi.org/10.1038/s41467-024-46103-3, 2024b.
- Cheng, Z., Wang, S., Qiao, L., Wang, H., Zhou, M., Fu, X., Lou, S., Luo, L., Jiang, J., Chen, C., Wang, X., and Hao, J.: Insights into extinction evolution during extreme low visibility events: Case study of Shanghai, China, Sci. Total Environ., 618, 793–803, https://doi.org/10.1016/j.scitotenv.2017.08.202, 2018.

- Cui, L., Li, R., Zhang, Y., Meng, Y., Fu, H., and Chen, J.: An observational study of nitrous acid (HONO) in Shanghai, China: The aerosol impact on HONO formation during the haze episodes, Sci. Total Environ., 630, 1057–1070, https://doi.org/10.1016/j.scitotenv.2018.02.063, 2018.
- Fu, X., Wang, T., Zhang, L., Li, Q., Wang, Z., Xia, M., Yun, H., Wang, W., Yu, C., Yue, D., Zhou, Y., Zheng, J., and Han, R.: The significant contribution of HONO to secondary pollutants during a severe winter pollution event in southern China, Atmos. Chem. Phys., 19, 1–14, https://doi.org/10.5194/acp-19-1-2019, 2019.
- Fu, X., Wang, T., Gao, J., Wang, P., Liu, Y., Wang, S., Zhao, B., and Xue, L.: Persistent Heavy Winter Nitrate Pollution Driven by Increased Photochemical Oxidants in Northern China, Environ. Sci. Technol., 54, 3881–3889, https://doi.org/10.1021/acs.est.9b07248, 2020.
- Gao, Z., Wang, Y., Gligorovski, S., Xue, C., Deng, L., Li, R., Duan, Y., Yin, S., Zhang, L., Zhang, Q., and Wu, D.: Explainable Machine Learning Reveals the Unknown Sources of Atmospheric HONO during COVID-19, ACS ES&T Air, 1, 1252– 1261, https://doi.org/10.1021/acsestair.4c00087, 2024.
- George, C., Ammann, M., D'Anna, B., Donaldson, D. J., and Nizkorodov, S. A.: Heterogeneous photochemistry in the atmosphere, Chem. Rev., 115, 4218–4258, https://doi.org/10.1021/cr500648z, 2015.
- Gu, R., Shen, H., Xue, L., Wang, T., Gao, J., Li, H., Liang, Y., Xia, M., Yu, C., Liu, Y., and Wang, W.: Investigating the sources of atmospheric nitrous acid (HONO) in the megacity of Beijing, China, Sci. Total Environ., 812, https://doi.org/10.1016/j.scitotenv.2021.152270, 2022.
- Gu, R. R., Zheng, P. G., Chen, T. S., Dong, C., Wang, Y. N., Liu, Y. M., Liu, Y. H., Luo, Y. Y., Han, G. X., Wang, X. F., Zhou, X. H., Wang, T., Wang, W. X., and Xue, L. K.: Atmospheric nitrous acid (HONO) at a rural coastal site in North China: Seasonal variations and effects of biomass burning, Atmos. Environ., 229, 11, https://doi.org/10.1016/j.atmosenv.2020.117429, 2020.
- Guha, S., Zhang, T., Kinney, P. L., and Henneman, L. R. F.: Fine particulate matter and ozone variability with regional and local meteorology in Beijing, China, Atmos. Environ., 338, 120793, https://doi.org/10.1016/j.atmosenv.2024.120793, 2024.
- Guo, S., Hu, M., Guo, Q., Zhang, X., Schauer, J. J., and Zhang, R.: Quantitative evaluation of emission controls on primary and secondary organic aerosol sources during Beijing 2008 Olympics, Atmos. Chem. Phys., 13, 8303–8314, https://doi.org/10.5194/acp-13-8303-2013, 2013.
- Guo, S., Hu, M., Zamora, M. L., Peng, J., Shang, D., Zheng, J., Du, Z., Wu, Z., Shao, M., Zeng, L., Molina, M. J., and Zhang, R.: Elucidating severe urban haze formation in China, P. Natl. Acad. Sci. USA, 111, 17373–17378, https://doi.org/10.1073/pnas.1419604111, 2014.
- Harrison, R. M., Peak, J. D., and Collins, G. M.: Tropospheric cycle of nitrous acid, J. Geophys. Res. Atmos., 101, 14429–14439, https://doi.org/10.1029/96jd00341, 1996.
- Heland, J., Kleffmann, J., Kurtenbach, R., and Wiesen, P.: A New Instrument To Measure Gaseous Nitrous Acid (HONO) in the Atmosphere, Environ. Sci. Technol., 35, 3207–3212, https://doi.org/10.1021/es000303t, 2001.
- Hou, S. Q., Tong, S. R., Ge, M. F., and An, J. L.: Comparison of atmospheric nitrous acid during severe haze and clean

- periods in Beijing, China, Atmos. Environ., 124, 199–206, https://doi.org/10.1016/j.atmosenv.2015.06.023, 2016.
- Huang, R. J., Zhang, Y., Bozzetti, C., Ho, K. F., Cao, J. J., Han, Y.,
 Daellenbach, K. R., Slowik, J. G., Platt, S. M., Canonaco, F., Zotter, P., Wolf, R., Pieber, S. M., Bruns, E. A., Crippa, M., Ciarelli, G., Piazzalunga, A., Schwikowski, M., Abbaszade, G., Schnelle-Kreis, J., Zimmermann, R., An, Z., Szidat, S., Baltensperger, U., El Haddad, I., and Prevot, A. S.: High secondary aerosol contribution to particulate pollution during haze events in China, Nature, 514, 218–222, https://doi.org/10.1038/nature13774, 2014.
- Huang, X. J., Tang, G. Q., Zhang, J. K., Liu, B. X., Liu, C., Zhang, J., Cong, L. L., Cheng, M. T., Yan, G. X., Gao, W. K., Wang, Y. H., and Wang, Y. S.: Characteristics of PM_{2.5} pollution in Beijing after the improvement of air quality, J. Environ. Sci., 100, 1–10, https://doi.org/10.1016/j.jes.2020.06.004, 2021.
- Huangfu, Y., Lima, N. M., O'Keeffe, P. T., Kirk, W. M., Lamb, B. K., Pressley, S. N., Lin, B., Cook, D. J., Walden, V. P., and Jobson, B. T.: Diel variation of formaldehyde levels and other VOCs in homes driven by temperature dependent infiltration and emission rates, Build. Environ., 159, 106153, https://doi.org/10.1016/j.buildenv.2019.05.031, 2019.
- Indarto, A.: Heterogeneous reactions of HONO formation from NO₂ and HNO₃: a review, Res. Chem. Intermed., 38, 1029– 1041, https://doi.org/10.1007/s11164-011-0439-z, 2011.
- Jenkin, M. E., Cox, R. A., and Williams, D. J.: Laboratory studies of the kinetics of formation of nitrous-acid from the thermalreaction of nitrogen-dioxide and water-vapor, Atmos. Environ., 22, 487–498, https://doi.org/10.1016/0004-6981(88)90194-1, 1988.
- Ji, Y., An, C., Tang, J., Li, J., Yan, X., Gao, X., Chu, W., Zhong, X., Shang, F., Li, J., Tan, L., Gao, R., Bi, F., and Li, H.: Causes Investigation of PM_{2.5} and O₃ Complex Pollution in a Typical Coastal City in the Bohai Bay Region of China in Autumn: Based on One-Month Continuous Intensive Observation and Model Simulation, Atmosphere, 15, https://doi.org/10.3390/atmos15010073, 2024.
- Jia, C., Tong, S., Zhang, W., Zhang, X., Li, W., Wang, Z., Wang, L., Liu, Z., Hu, B., Zhao, P., and Ge, M.: Pollution characteristics and potential sources of nitrous acid (HONO) in early autumn 2018 of Beijing, Sci. Total Environ., 735, 139317, https://doi.org/10.1016/j.scitotenv.2020.139317, 2020.
- Jiang, Y., Xia, M., Xue, L., Wang, X., Zhong, X., Liu, Y., Kulmala, M., Ma, T., Wang, J., Wang, Y., Gao, J., and Wang, T.: Quantifying HONO Production from Nitrate Photolysis in a Polluted Atmosphere, Environ. Sci. Technol., https://doi.org/10.1021/acs.est.4c06061, 2024.
- Kebede, M. A., Bish, D. L., Losovyj, Y., Engelhard, M. H., and Raff, J. D.: The Role of Iron-Bearing Minerals in NO₂ to HONO Conversion on Soil Surfaces, Environ. Sci. Technol., 50, 8649–8660, https://doi.org/10.1021/acs.est.6b01915, 2016.
- Kim, S., VandenBoer, T. C., Young, C. J., Riedel, T. P., Thornton, J. A., Swarthout, B., Sive, B., Lerner, B., Gilman, J. B., Warneke, C., Roberts, J. M., Guenther, A., Wagner, N. L., Dube, W. P., Williams, E., and Brown, S. S.: The primary and recycling sources of OH during the NACHTT-2011 campaign: HONO as an important OH primary source in the wintertime, J. Geophys. Res. Atmos., 119, 6886–6896, https://doi.org/10.1002/2013jd019784, 2014.

- Kurtenbach, R., Becker, K. H., Gomes, J. A. G., Kleffmann, J., Lorzer, J. C., Spittler, M., Wiesen, P., Ackermann, R., Geyer, A., and Platt, U.: Investigations of emissions and heterogeneous formation of HONO in a road traffic tunnel, Atmos. Environ., 35, 3385–3394, https://doi.org/10.1016/s1352-2310(01)00138-8, 2001.
- Kurtenbach, R., Kleffmann, J., Niedojadlo, A., and Wiesen, P.: Primary NO₂ emissions and their impact on air quality in traffic environments in Germany, Environ. Sci. Eur., 24, 21, https://doi.org/10.1186/2190-4715-24-21, 2012.
- Lee, J. D., Whalley, L. K., Heard, D. E., Stone, D., Dunmore, R. E., Hamilton, J. F., Young, D. E., Allan, J. D., Laufs, S., and Kleffmann, J.: Detailed budget analysis of HONO in central London reveals a missing daytime source, Atmos. Chem. Phys., 16, 2747–2764, https://doi.org/10.5194/acp-16-2747-2016, 2016.
- Li, D., Xue, L., Wen, L., Wang, X., Chen, T., Mellouki, A., Chen, J., and Wang, W.: Characteristics and sources of nitrous acid in an urban atmosphere of northern China: Results from 1-yr continuous observations, Atmos. Environ., 182, 296–306, https://doi.org/10.1016/j.atmosenv.2018.03.033, 2018a.
- Li, L., Duan, Z., Li, H., Zhu, C., Henkelman, G., Francisco, J. S., and Zeng, X. C.: Formation of HONO from the NH₃-promoted hydrolysis of NO₂ dimers in the atmosphere, P. Natl. Acad. Sci. USA, 115, 7236–7241, https://doi.org/10.1073/pnas.1807719115, 2018b.
- Li, Q., Su, G., Li, C., Liu, P., Zhao, X., Zhang, C., Sun, X., Mu, Y., Wu, M., Wang, Q., and Sun, B.: An investigation into the role of VOCs in SOA and ozone production in Beijing, China, Sci. Total Environ., 720, 137536, https://doi.org/10.1016/j.scitotenv.2020.137536, 2020.
- Li, X., Brauers, T., Häseler, R., Bohn, B., Fuchs, H., Hofzumahaus, A., Holland, F., Lou, S., Lu, K. D., Rohrer, F., Hu, M., Zeng, L. M., Zhang, Y. H., Garland, R. M., Su, H., Nowak, A., Wiedensohler, A., Takegawa, N., Shao, M., and Wahner, A.: Exploring the atmospheric chemistry of nitrous acid (HONO) at a rural site in Southern China, Atmos. Chem. Phys., 12, 1497–1513, https://doi.org/10.5194/acp-12-1497-2012, 2012.
- Li, X. D., Jin, L., and Kan, H. D.: Air pollution: a global problem needs local fixes, Nature, 570, 437–439, https://doi.org/10.1038/d41586-019-01960-7, 2019.
- Li, Y., Wang, X., Wu, Z., Li, L., Wang, C., Li, H., Zhang, X., Zhang, Y., Li, J., Gao, R., Xue, L., Mellouki, A., Ren, Y., and Zhang, Q.: Atmospheric nitrous acid (HONO) in an alternate process of haze pollution and ozone pollution in urban Beijing in summertime: Variations, sources and contribution to atmospheric photochemistry, Atmos. Res., 260, https://doi.org/10.1016/j.atmosres.2021.105689, 2021.
- Lian, C., Wang, W., Chen, Y., Zhang, Y., Zhang, J., Liu, Y., Fan, X., Li, C., Zhan, J., Lin, Z., Hua, C., Zhang, W., Liu, M., Li, J., Wang, X., An, J., and Ge, M.: Long-term winter observation of nitrous acid in the urban area of Beijing, J. Environ. Sci. China, 114, 334–342, https://doi.org/10.1016/j.jes.2021.09.010, 2022.
- Liao, S., Zhang, J., Yu, F., Zhu, M., Liu, J., Ou, J., Dong, H., Sha, Q., Zhong, Z., Xie, Y., Luo, H., Zhang, L., and Zheng, J.: High Gaseous Nitrous Acid (HONO) Emissions from Light-Duty Diesel Vehicles, Environ. Sci. Technol., 55, 200–208, https://doi.org/10.1021/acs.est.0c05599, 2021.
- Lin, D., Tong, S., Zhang, W., Li, W., Li, F., Jia, C., Zhang, G., Chen, M., Zhang, X., Wang, Z., Ge, M., and He, X.: Formation mech-

- anisms of nitrous acid (HONO) during the haze and non-haze periods in Beijing, China, J. Environ. Sci. China, 114, 343–353, https://doi.org/10.1016/j.jes.2021.09.013, 2022.
- Liu, J., Li, S., Mekic, M., Jiang, H., Zhou, W., Loisel, G., Song, W., Wang, X., and Gligorovski, S.: Photoenhanced Uptake of NO₂ and HONO Formation on Real Urban Grime, Environ. Sci. Technol. Lett., 6, 413–417, https://doi.org/10.1021/acs.estlett.9b00308, 2019a.
- Liu, J., Liu, Z., Ma, Z., Yang, S., Yao, D., Zhao, S., Hu, B., Tang, G., Sun, J., Cheng, M., Xu, Z., and Wang, Y.: Detailed budget analysis of HONO in Beijing, China: Implication on atmosphere oxidation capacity in polluted megacity, Atmos. Environ., 244, https://doi.org/10.1016/j.atmosenv.2020.117957, 2021.
- Liu, P., Ye, C., Xue, C., Zhang, C., Mu, Y., and Sun, X.: Formation mechanisms of atmospheric nitrate and sulfate during the winter haze pollution periods in Beijing: gas-phase, heterogeneous and aqueous-phase chemistry, Atmos. Chem. Phys., 20, 4153–4165, https://doi.org/10.5194/acp-20-4153-2020, 2020.
- Liu, Y., Lu, K., Li, X., Dong, H., Tan, Z., Wang, H., Zou, Q., Wu, Y., Zeng, L., Hu, M., Min, K. E., Kecorius, S., Wiedensohler, A., and Zhang, Y.: A comprehensive model test of the HONO sources constrained to field measurements at rural North China Plain, Environ. Sci. Technol., 53, 3517–3525, https://doi.org/10.1021/acs.est.8b06367, 2019b.
- Liu, Y. C., Wu, Z. J., Qiu, Y. T., Tian, P., Liu, Q., Chen, Y., Song, M., and Hu, M.: Enhanced Nitrate Fraction: Enabling Urban Aerosol Particles to Remain in a Liquid State at Reduced Relative Humidity, Geophys. Res. Lett., 50, https://doi.org/10.1029/2023g1105505, 2023.
- Lu, X. C., Wang, Y. H., Li, J. F., Shen, L., and Fung, J. C. H.: Evidence of heterogeneous HONO formation from aerosols and the regional photochemical impact of this HONO source, Environ. Res. Lett., 13, https://doi.org/10.1088/1748-9326/aae492, 2018.
- Ndour, M., D'Anna, B., George, C., Ka, O., Balkanski, Y., Kleffmann, J., Stemmler, K., and Ammann, M.: Photoenhanced uptake of NO₂ on mineral dust: Laboratory experiments and model simulations, Geophys. Res. Lett., 35, https://doi.org/10.1029/2007g1032006, 2008.
- Nie, W., Ding, A. J., Xie, Y. N., Xu, Z., Mao, H., Kerminen, V.-M., Zheng, L. F., Qi, X. M., Huang, X., Yang, X.-Q., Sun, J. N., Herrmann, E., Petäjä, T., Kulmala, M., and Fu, C. B.: Influence of biomass burning plumes on HONO chemistry in eastern China, Atmos. Chem. Phys., 15, 1147–1159, https://doi.org/10.5194/acp-15-1147-2015, 2015.
- Pagsberg, P., Bjergbakke, E., Ratajczak, E., and Sillesen, A.: Kinetics of the gas phase reaction OH+NO(+M)→HONO(+M) and the determination of the UV absorption cross sections of HONO, Chem. Phys. Lett., 272, 383–390, https://doi.org/10.1016/s0009-2614(97)00576-9, 1997.
- Qi, L., Yin, J., Li, J., and Duan, X.: Detecting causal relationships between fine particles and ozone based on observations in four typical cities of China, Environ. Res. Lett., 19, https://doi.org/10.1088/1748-9326/ad376d, 2024.
- Qin, M., Xie, P., Su, H., Gu, J., Peng, F., Li, S., Zeng, L., Liu, J., Liu, W., and Zhang, Y.: An observational study of the HONO-NO₂ coupling at an urban site in Guangzhou City, South China, Atmos. Environ., 43, 5731–5742, https://doi.org/10.1016/j.atmosenv.2009.08.017, 2009.

- Qin, M., She, Y., Wang, M., Wang, H., Chang, Y., Tan, Z., An, J., Huang, J., Yuan, Z., Lu, J., Wang, Q., Liu, C., Liu, Z., Xie, X., Li, J., Liao, H., Pye, H. O. T., Huang, C., Guo, S., Hu, M., Zhang, Y., Jacob, D. J., and Hu, J.: Increased urban ozone in heatwaves due to temperature-induced emissions of anthropogenic volatile organic compounds, Nat. Geosci., 18, 50–56, https://doi.org/10.1038/s41561-024-01608-w, 2025.
- Qu, Y., Wang, T., Yuan, C., Wu, H., Gao, L., Huang, C., Li, Y., Li, M., and Xie, M.: The underlying mechanisms of PM_{2.5} and O₃ synergistic pollution in East China: Photochemical and heterogeneous interactions, Sci. Total Environ., 873, https://doi.org/10.1016/j.scitotenv.2023.162434, 2023.
- Shen, H., Xue, L., Fan, G., Xu, H., Zhang, Z., Pan, G., Wang, T., and Wang, W.: Trace Metals Reveal Significant Contribution of Coal Combustion to Winter Haze Pollution in Northern China, ACS ES&T Air, 1, 714–724, https://doi.org/10.1021/acsestair.4c00050, 2024.
- Shi, G., Yang, F., Zhang, L., Zhao, T., and Hu, J.: Impact of Atmospheric Circulation and Meteorological Parameters on Wintertime Atmospheric Extinction in Chengdu and Chongqing of Southwest China during 2001–2016, Aerosol Air Qual. Res., 19, 1538–1554, https://doi.org/10.4209/aaqr.2018.09.0336, 2019.
- Shi, X., Ge, Y., Zheng, J., Ma, Y., Ren, X., and Zhang, Y.: Budget of nitrous acid and its impacts on atmospheric oxidative capacity at an urban site in the central Yangtze River Delta region of China, Atmos. Environ., 238, https://doi.org/10.1016/j.atmosenv.2020.117725, 2020.
- Slater, E. J., Whalley, L. K., Woodward-Massey, R., Ye, C., Lee, J. D., Squires, F., Hopkins, J. R., Dunmore, R. E., Shaw, M., Hamilton, J. F., Lewis, A. C., Crilley, L. R., Kramer, L., Bloss, W., Vu, T., Sun, Y., Xu, W., Yue, S., Ren, L., Acton, W. J. F., Hewitt, C. N., Wang, X., Fu, P., and Heard, D. E.: Elevated levels of OH observed in haze events during winter-time in central Beijing, Atmos. Chem. Phys., 20, 14847–14871, https://doi.org/10.5194/acp-20-14847-2020, 2020.
- Spataro, F. and Ianniello, A.: Sources of atmospheric nitrous acid: state of the science, current research needs, and future prospects, J. Air Waste Manag. Assoc., 64, 1232–1250, https://doi.org/10.1080/10962247.2014.952846, 2014.
- Spataro, F., Ianniello, A., Esposito, G., Allegrini, I., Zhu, T., and Hu, M.: Occurrence of atmospheric nitrous acid in the urban area of Beijing (China), Sci. Total Environ., 447, 210–224, https://doi.org/10.1016/j.scitotenv.2012.12.065, 2013.
- Stutz, J., Alicke, B., Ackermann, R., Geyer, A., Wang, S. H., White, A. B., Williams, E. J., Spicer, C. W., and Fast, J. D.: Relative humidity dependence of HONO chemistry in urban areas, J. Geophys. Res. Atmos., 109, https://doi.org/10.1029/2003jd004135, 2004.
- Su, H., Cheng, Y. F., Cheng, P., Zhang, Y. H., Dong, S., Zeng, L. M., Wang, X., Slanina, J., Shao, M., and Wiedensohler, A.: Observation of nighttime nitrous acid (HONO) formation at a nonurban site during PRIDE-PRD2004 in China, Atmos. Environ., 42, 6219–6232, https://doi.org/10.1016/j.atmosenv.2008.04.006, 2008.
- Sun, Y., Wang, Y., and Zhang, C.: Vertical observations and analysis of PM_{2.5}, O₃, and NO_x at Beijing and Tianjin from towers during summer and Autumn 2006, Adv. Atmos. Sci., 27, 123–136, https://doi.org/10.1007/s00376-009-8154-z, 2009.

- Sun, Y., Jiang, Q., Wang, Z., Fu, P., Li, J., Yang, T., and Yin, Y.: Investigation of the sources and evolution processes of severe haze pollution in Beijing in January 2013, J. Geophys. Res. Atmos., 119, 4380–4398, https://doi.org/10.1002/2014jd021641, 2014.
- Tan, Z., Feng, M., Liu, H., Luo, Y., Li, W., Song, D., Tan, Q., Ma, X., Lu, K., and Zhang, Y.: Atmospheric Oxidation Capacity Elevated during 2020 Spring Lockdown in Chengdu, China: Lessons for Future Secondary Pollution Control, Environ. Sci. Technol., https://doi.org/10.1021/acs.est.3c08761, 2024.
- Tao, C., Zhang, Q., Huo, S., Ren, Y., Han, S., Wang, Q., and Wang, W.: PM_{2.5} pollution modulates the response of ozone formation to VOC emitted from various sources: Insights from machine learning, Sci. Total Environ., 916, https://doi.org/10.1016/j.scitotenv.2024.170009, 2024.
- Theys, N., Volkamer, R., Müller, J. F., Zarzana, K. J., Kille, N., Clarisse, L., De Smedt, I., Lerot, C., Finkenzeller, H., Hendrick, F., Koenig, T. K., Lee, C. F., Knote, C., Yu, H., and Van Roozendael, M.: Global nitrous acid emissions and levels of regional oxidants enhanced by wildfires, Nat. Geosci., https://doi.org/10.1038/s41561-020-0637-7, 2020.
- Tie, X., Long, X., Li, G., Zhao, S., Cao, J., and Xu, J.: Ozone enhancement due to the photodissociation of nitrous acid in eastern China, Atmos. Chem. Phys., 19, 11267–11278, https://doi.org/10.5194/acp-19-11267-2019, 2019.
- Tong, S., Hou, S., Zhang, Y., Chu, B., Liu, Y., He, H., Zhao, P., and Ge, M.: Comparisons of measured nitrous acid (HONO) concentrations in a pollution period at urban and suburban Beijing, in autumn of 2014, Sci. China Chem., 58, 1393–1402, https://doi.org/10.1007/s11426-015-5454-2, 2015.
- Tong, S. R., Hou, S. Q., Zhang, Y., Chu, B. W., Liu, Y. C., He, H., Zhao, P. S., and Ge, M. F.: Exploring the nitrous acid (HONO) formation mechanism in winter Beijing: direct emissions and heterogeneous production in urban and suburban areas, Faraday Discuss., 189, 213–230, https://doi.org/10.1039/C5FD00163C, 2016.
- Villena, G., Bejan, I., Kurtenbach, R., Wiesen, P., and Kleffmann, J.: Interferences of commercial NO₂ instruments in the urban atmosphere and in a smog chamber, Atmos. Meas. Tech., 5, 149–159, https://doi.org/10.5194/amt-5-149-2012, 2012.
- Wall, K. J. and Harris, G. W.: Uptake of nitrogen dioxide (NO₂) on acidic aqueous humic acid (HA) solutions as a missing daytime nitrous acid (HONO) surface source, J. Atmos. Chem., 74, 283–321, https://doi.org/10.1007/s10874-016-9342-8, 2017.
- Wang, J., Zhang, X., Guo, J., Wang, Z., and Zhang, M.: Observation of nitrous acid (HONO) in Beijing, China: Seasonal variation, nocturnal formation and daytime budget, Sci. Total Environ., 587–588, 350–359, https://doi.org/10.1016/j.scitotenv.2017.02.159, 2017.
- Wang, J., Tang, D., Shang, L., and Lansana, D. D.: Impact of air pollution perception on environmental governance satisfaction, Humanit. Soc. Sci. Commun., 11, https://doi.org/10.1057/s41599-024-03484-6, 2024.
- Wang, W., Li, X., Cheng, Y., Parrish, D. D., Ni, R., Tan, Z., Liu, Y., Lu, S., Wu, Y., Chen, S., Lu, K., Hu, M., Zeng, L., Shao, M., Huang, C., Tian, X., Leung, K. M., Chen, L., Fan, M., Zhang, Q., Rohrer, F., Wahner, A., Pöschl, U., Su, H., and Zhang, Y.: Ozone pollution mitigation strategy informed by long-term trends of atmospheric oxidation capacity, Nat. Geosci., 17, 20–25, https://doi.org/10.1038/s41561-023-01334-9, 2023.

- Wolfe, G. M., Marvin, M. R., Roberts, S. J., Travis, K. R., and Liao, J.: The Framework for 0-D Atmospheric Modeling (F0AM) v3.1, Geosci. Model Dev., 9, 3309–3319, https://doi.org/10.5194/gmd-9-3309-2016, 2016.
- Wu, D., Zhang, J., Wang, M., An, J., Wang, R., Haider, H., Xu-Ri, Huang, Y., Zhang, Q., Zhou, F., Tian, H., Zhang, X., Deng, L., Pan, Y., Chen, X., Yu, Y., Hu, C., Wang, R., Song, Y., Gao, Z., Wang, Y., Hou, L., and Liu, M.: Global and Regional Patterns of Soil Nitrous Acid Emissions and Their Acceleration of Rural Photochemical Reactions, J. Geophys. Res. Atmos., 127, https://doi.org/10.1029/2021JD036379, 2022a.
- Wu, X., Xin, J., Zhang, W., Gao, W., Ma, Y., Ma, Y., Wen, T., Liu, Z., Hu, B., Wang, Y., and Wang, L.: Variation characteristics of air combined pollution in Beijing City, Atmos. Res., 274, https://doi.org/10.1016/j.atmosres.2022.106197, 2022b.
- Xiao, H. W., Chen, T. S., Zhang, Q. J., Wang, R., Xiao, H., Xu, Y., Guan, W. K., Long, A. M., and Xiao, H. Y.: Changes in the Dominant Contributions of Nitrate Formation and Sources During Haze Episodes: Insights From Dual Isotopic Evidence, J. Geophys. Res. Atmos., 130, https://doi.org/10.1029/2024jd042175, 2025.
- Xu, Q., Wang, S., Jiang, J., Bhattarai, N., Li, X., Chang, X., Qiu, X., Zheng, M., Hua, Y., and Hao, J.: Nitrate dominates the chemical composition of PM_{2.5} during haze event in Beijing, China, Sci. Total Environ., 689, 1293–1303, https://doi.org/10.1016/j.scitotenv.2019.06.294, 2019.
- Xu, Z., Wang, T., Wu, J., Xue, L., Chan, J., Zha, Q., Zhou, S., Louie, P. K. K., and Luk, C. W. Y.: Nitrous acid (HONO) in a polluted subtropical atmosphere: Seasonal variability, direct vehicle emissions and heterogeneous production at ground surface, Atmos. Environ., 106, 100–109, https://doi.org/10.1016/j.atmosenv.2015.01.061, 2015.
- Xuan, H., Zhao, Y., Ma, Q., Chen, T., Liu, J., Wang, Y., Liu, C., Wang, Y., Liu, Y., Mu, Y., and He, H.: Formation mechanisms and atmospheric implications of summertime nitrous acid (HONO) during clean, ozone pollution and double high-level PM_{2.5} and O₃ pollution periods in Beijing, Sci. Total Environ., 857, 159538, https://doi.org/10.1016/j.scitotenv.2022.159538, 2023
- Xuan, H., Liu, J., Zhao, Y., Cao, Q., Chen, T., Wang, Y., Liu, Z., Sun, X., Li, H., Zhang, P., Chu, B., Ma, Q., and He, H.: Relative humidity driven nocturnal HONO formation mechanism in autumn haze events of Beijing, npj Clim. Atmos. Sci., 7, https://doi.org/10.1038/s41612-024-00745-8, 2024.
- Xue, L., Gu, R., Wang, T., Wang, X., Saunders, S., Blake, D., Louie, P. K. K., Luk, C. W. Y., Simpson, I., Xu, Z., Wang, Z., Gao, Y., Lee, S., Mellouki, A., and Wang, W.: Oxidative capacity and radical chemistry in the polluted atmosphere of Hong Kong and Pearl River Delta region: analysis of a severe photochemical smog episode, Atmos. Chem. Phys., 16, 9891–9903, https://doi.org/10.5194/acp-16-9891-2016, 2016.
- Xue, C., Zhang, C., Ye, C., Liu, P., Catoire, V., Krysztofiak, G., Chen, H., Ren, Y., Zhao, X., Wang, J., Zhang, F., Zhang, C., Zhang, J., An, J., Wang, T., Chen, J., Kleffmann, J., Mellouki, A., and Mu, Y.: HONO Budget and Its Role in Nitrate Formation in the Rural North China Plain, Environ. Sci. Technol., 54, 11048–11057, https://doi.org/10.1021/acs.est.0c01832, 2020.
- Xue, C., Ye, C., Zhang, C., Catoire, V., Liu, P., Gu, R., Zhang, J., Ma, Z., Zhao, X., Zhang, W., Ren, Y., Krysztofiak, G., Tong,

- S., Xue, L., An, J., Ge, M., Mellouki, A., and Mu, Y.: Evidence for Strong HONO Emission from Fertilized Agricultural Fields and its Remarkable Impact on Regional O₃ Pollution in the Summer North China Plain, ACS Earth Space Chem., https://doi.org/10.1021/acsearthspacechem.0c00314, 2021.
- Xue, C., Ye, C., Kleffmann, J., Zhang, W., He, X., Liu, P., Zhang, C., Zhao, X., Liu, C., Ma, Z., Liu, J., Wang, J., Lu, K., Catoire, V., Mellouki, A., and Mu, Y.: Atmospheric measurements at Mt. Tai Part II: HONO budget and radical (RO_x + NO₃) chemistry in the lower boundary layer, Atmos. Chem. Phys., 22, 1035–1057, https://doi.org/10.5194/acp-22-1035-2022, 2022.
- Xue, C., Ye, C., Lu, K., Liu, P., Zhang, C., Su, H., Bao, F., Cheng, Y., Wang, W., Liu, Y., Catoire, V., Ma, Z., Zhao, X., Song, Y., Ma, X., McGillen, M. R., Mellouki, A., Mu, Y., and Zhang, Y.: Reducing Soil-Emitted Nitrous Acid as a Feasible Strategy for Tackling Ozone Pollution, Environ. Sci. Technol., https://doi.org/10.1021/acs.est.4c01070, 2024.
- Yan, R., Yu, S., Zhang, Q., Li, P., Wang, S., Chen, B., and Liu, W.: A heavy haze episode in Beijing in February of 2014: Characteristics, origins and implications, Atmos. Pollut. Res., 6, 867–876, https://doi.org/10.5094/apr.2015.096, 2015.
- Yang, W., Han, C., Zhang, T., Tang, N., Yang, H., and Xue, X.: Heterogeneous photochemical uptake of NO₂ on the soil surface as an important ground-level HONO source, Environ. Pollut., 271, 116289, https://doi.org/10.1016/j.envpol.2020.116289, 2021.
- Ye, C., Zhang, N., Gao, H., and Zhou, X.: Photolysis of Particulate Nitrate as a Source of HONO and NO_x, Environ. Sci. Technol., 51, 6849–6856, https://doi.org/10.1021/acs.est.7b00387, 2017.
- Ye, C., Lu, K., Ma, X., Qiu, W., Li, S., Yang, X., Xue, C., Zhai, T., Liu, Y., Li, X., Li, Y., Wang, H., Tan, Z., Chen, X., Dong, H., Zeng, L., Hu, M., and Zhang, Y.: HONO chemistry at a suburban site during the EXPLORE-YRD campaign in 2018: formation mechanisms and impacts on O₃ production, Atmos. Chem. Phys., 23, 15455–15472, https://doi.org/10.5194/acp-23-15455-2023, 2023.
- Yin, X., Tang, F., Huang, Z., Liao, S., Sha, Q., Cheng, P., Lu, M., Li, Z., Yu, F., Xu, Y., Shao, M., and Zheng, J.: Developing a model-ready highly resolved HONO emission inventory in Guangdong using domestic measured emission factors, Sci. Total Environ., 899, https://doi.org/10.1016/j.scitotenv.2023.165737, 2023.
- Yu, C., Wang, Z., Ma, Q., Xue, L., George, C., and Wang, T.: Measurement of heterogeneous uptake of NO2 on inorganic particles, sea water and urban grime, J. Environ. Sci., 106, 124–135, https://doi.org/10.1016/j.jes.2021.01.018, 2021.
- Yu, Y., Cheng, P., Li, H., Yang, W., Han, B., Song, W., Hu, W., Wang, X., Yuan, B., Shao, M., Huang, Z., Li, Z., Zheng, J., Wang, H., and Yu, X.: Budget of nitrous acid (HONO) at an urban site in the fall season of Guangzhou, China, Atmos. Chem. Phys., 22, 8951–8971, https://doi.org/10.5194/acp-22-8951-2022, 2022.
- Yun, H., Wang, Z., Zha, Q. Z., Wang, W. H., Xue, L. K., Zhang, L., Li, Q. Y., Cui, L., Lee, S. C., Poon, S. C. N., and Wang, T.: Nitrous acid in a street canyon environment: Sources and contributions to local oxidation capacity, Atmos. Environ., 167, 223–234, https://doi.org/10.1016/j.atmosenv.2017.08.018, 2017.
- Zhai, M., Tong, S., Zhang, W., Zhang, H., Li, X., Wang, X., and Ge, M.: Measurement report: Anthropogenic activities reduction suppresses HONO formation: direct evidence for Secondary Pollution control, Zenodo [data set], https://doi.org/10.5281/zenodo.16083849, 2025.

- Zhai, S., Jacob, D. J., Wang, X., Liu, Z., Wen, T., Shah, V., Li, K., Moch, J. M., Bates, K. H., Song, S., Shen, L., Zhang, Y., Luo, G., Yu, F., Sun, Y., Wang, L., Qi, M., Tao, J., Gui, K., Xu, H., Zhang, Q., Zhao, T., Wang, Y., Lee, H. C., Choi, H., and Liao, H.: Control of particulate nitrate air pollution in China, Nat. Geosci., 14, 389–395, https://doi.org/10.1038/s41561-021-00726-z, 2021.
- Zhang, D. Y., Liu, J. J., and Li, B. J.: Tackling Air Pollution in China-What do We Learn from the Great Smog of 1950s in LONDON, Sustainability, 6, 5322–5338, https://doi.org/10.3390/su6085322, 2014.
- Zhang, H., Wang, S., Hao, J., Wang, X., Wang, S., Chai, F., and Li, M.: Air pollution and control action in Beijing, J. Clean. Prod., 112, 1519–1527, https://doi.org/10.1016/j.jclepro.2015.04.092, 2016.
- Zhang, J., An, J., Qu, Y., Liu, X., and Chen, Y.: Impacts of potential HONO sources on the concentrations of oxidants and secondary organic aerosols in the Beijing-Tianjin-Hebei region of China, Sci. Total Environ., 647, 836–852, https://doi.org/10.1016/j.scitotenv.2018.08.030, 2019a.
- Zhang, J., Lian, C., Wang, W., Ge, M., Guo, Y., Ran, H., Zhang, Y., Zheng, F., Fan, X., Yan, C., Daellenbach, K. R., Liu, Y., Kulmala, M., and An, J.: Amplified role of potential HONO sources in O₃ formation in North China Plain during autumn haze aggravating processes, Atmos. Chem. Phys., 22, 3275–3302, https://doi.org/10.5194/acp-22-3275-2022, 2022a.
- Zhang, R., Wang, G., Guo, S., Zamora, M. L., Ying, Q., Lin, Y., Wang, W., Hu, M., and Wang, Y.: Formation of urban fine particulate matter, Chem. Rev., 115, 3803–3855, https://doi.org/10.1021/acs.chemrev.5b00067, 2015.
- Zhang, S., Li, G., Ma, N., He, Y., Zhu, S., Pan, X., Dong, W., Zhang, Y., Luo, Q., Ditas, J., Kuhn, U., Zhang, Y., Yuan, B., Wang, Z., Cheng, P., Hong, J., Tao, J., Xu, W., Kuang, Y., Wang, Q., Sun, Y., Zhou, G., Cheng, Y., and Su, H.: Exploring HONO formation and its role in driving secondary pollutants formation during winter in the North China Plain, J. Environ. Sci., 132, 83–97, https://doi.org/10.1016/j.jes.2022.09.034, 2023a.
- Zhang, W., Tong, S., Ge, M., An, J., Shi, Z., Hou, S., Xia, K., Qu, Y., Zhang, H., Chu, B., Sun, Y., and He, H.: Variations and sources of nitrous acid (HONO) during a severe pollution episode in Beijing in winter 2016, Sci. Total Environ., 648, 253–262, https://doi.org/10.1016/j.scitotenv.2018.08.133, 2019b.
- Zhang, W., Tong, S., Jia, C., Wang, L., Liu, B., Tang, G., Ji, D., Hu, B., Liu, Z., Li, W., Wang, Z., Liu, Y., Wang, Y., and Ge, M.: Different HONO Sources for Three Layers at the Urban Area of Beijing, Environ. Sci. Technol., 54, 12870–12880, https://doi.org/10.1021/acs.est.0c02146, 2020.

- Zhang, W., Tong, S., Jia, C., Ge, M., Ji, D., Zhang, C., Liu, P., Zhao, X., Mu, Y., Hu, B., Wang, L., Tang, G., Li, X., Li, W., and Wang, Z.: Effect of Different Combustion Processes on Atmospheric Nitrous Acid Formation Mechanisms: A Winter Comparative Observation in Urban, Suburban and Rural Areas of the North China Plain, Environ. Sci. Technol., 56, 4828–4837, https://doi.org/10.1021/acs.est.1c07784, 2022b.
- Zhang, W., Tong, S., Lin, D., Li, F., Zhang, X., Wang, L., Ji, D., Tang, G., Liu, Z., Hu, B., and Ge, M.: Atmospheric chemistry of nitrous acid and its effects on hydroxyl radical and ozone at the urban area of Beijing in early spring 2021, Environ. Pollut., 316, 120710, https://doi.org/10.1016/j.envpol.2022.120710, 2023b.
- Zhang, X., Tong, S., Jia, C., Zhang, W., Li, J., Wang, W., Sun, Y., Wang, X., Wang, L., Ji, D., Wang, L., Zhao, P., Tang, G., Xin, J., Li, A., and Ge, M.: The Levels and Sources of Nitrous Acid (HONO) in Winter of Beijing and Sanmenxia, J. Geophys. Res. Atmos., 127, https://doi.org/10.1029/2021jd036278, 2022c.
- Zhang, X., Tong, S., Jia, C., Zhang, W., Wang, Z., Tang, G., Hu, B., Liu, Z., Wang, L., Zhao, P., Pan, Y., and Ge, M.: Elucidating HONO formation mechanism and its essential contribution to OH during haze events, npj Clim. Atmos. Sci., 6, https://doi.org/10.1038/s41612-023-00371-w, 2023c.
- Zhang, Z., Xu, W., Zeng, S., Liu, Y., Liu, T., Zhang, Y., Du, A., Li, Y., Zhang, N., Wang, J., Aruffo, E., Han, P., Li, J., Wang, Z., and Sun, Y.: Secondary Organic Aerosol Formation from Ambient Air in Summer in Urban Beijing: Contribution of S/IVOCs and Impacts of Heat Waves, Environ. Sci. Technol. Lett., 11, 738–745, https://doi.org/10.1021/acs.estlett.4c00415, 2024.
- Zheng, G. J., Duan, F. K., Su, H., Ma, Y. L., Cheng, Y., Zheng, B., Zhang, Q., Huang, T., Kimoto, T., Chang, D., Pöschl, U., Cheng, Y. F., and He, K. B.: Exploring the severe winter haze in Beijing: the impact of synoptic weather, regional transport and heterogeneous reactions, Atmos. Chem. Phys., 15, 2969–2983, https://doi.org/10.5194/acp-15-2969-2015, 2015.
- Zong, Z., Tian, C., Sun, Z., Tan, Y., Shi, Y., Liu, X., Li, J., Fang, Y., Chen, Y., Ma, Y., Gao, H., Zhang, G., and Wang, T.: Long-Term Evolution of Particulate Nitrate Pollution in North China: Isotopic Evidence From 10 Offshore Cruises in the Bohai Sea From 2014 to 2019, J. Geophys. Res. Atmos., 127, https://doi.org/10.1029/2022jd036567, 2022.